

Experimental Synthesis of Theoretically Predicted Multivalent Ternary Nitride Materials

Andriy Zakutayev,* Sage R. Bauers, and Stephan Lany



Cite This: *Chem. Mater.* 2022, 34, 1418–1438



Read Online

ACCESS |



Metrics & More



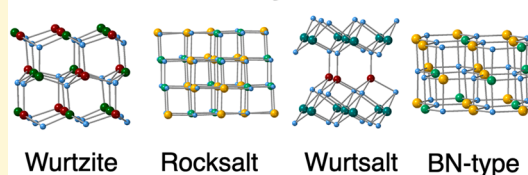
Article Recommendations



Supporting Information

ABSTRACT: Multivalent ternary nitride materials, which combine two metal cations with a nitrogen anion in equal amounts and charge balanced stoichiometry, tend to have relatively simple structures and promising properties for a broad range of applications. Historically, discovery of such new nitrides has been a bulk synthesis endeavor, following chemical intuition. In the past decade experimental synthesis of theoretically predicted materials, including as thin films, has changed this approach. In this perspective, we discuss progress in the experimental synthesis of theoretically predicted multivalent ternary nitrides, with the focus on Zn- and Mg-based materials. First-principles theoretical calculations predicted structures and properties of many new Zn–M–N and Mg–M–N materials and offered insights into the effects of cation ordering. Thin film and bulk experiments were used to synthesize some of these predicted multivalent ternary nitride compounds such as Zn₃MoN₄, Zn₂SbN₃, and Zn₂NbN₃, as well as MgZrN₂, Mg₂NbN₃, and Mg₂SbN₃, and many others. These multivalent ternary nitride success stories should inspire experimental synthesis of other underexplored materials predicted by theoretical calculations.

Multivalent Ternary Nitride Materials



1. INTRODUCTION

For more than a century, solid state chemistry has typically progressed by experimentally synthesizing materials, determining the resulting phases by characterizing their chemical composition and crystal structure, and sometimes following on with additional measurements or calculations to explain the physical origins of their properties. This mode of operation has placed the entirety of the scientific method of new materials discovery in hands of experimental chemists, in contrast to other fields, such as physics, where theory often drives experiments. To expand the materials palette, experimental material scientists made observations about materials, formulated hypotheses about the next material to investigate, and then tested these hypotheses by performing new synthesis and characterization experiments, while theoretical scientists helped explain some of the experimental results. One of the standout achievements of this relatively slow but deliberate, ongoing, and useful process over the past century is the creation of crystallographic structure databases¹ that summarize experimental observations in a structured format. The crystal structure information contained in these databases has democratized the scientific method in the field of materials science by providing large quantities of input information for first-principles theoretical calculations. Such calculations enabled theorists to formulate hypotheses about which materials to try synthesizing next, based on their thermochemical stability and physical properties predicted using density functional theory (DFT).² The parallel advent of high-performance computing resources and efficient implementations of the DFT algorithms³ has resulted in computational property databases^{4–6} containing many more predictions/hypotheses than is feasible to experimentally test with existing

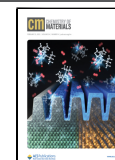
equipment. This progress has changed the materials science paradigm from theoretical explanations of experiment results to experimental synthesis of theoretical predictions^{7,8} or tight iterative collaboration between experiments and theory^{9–11} in the spirit of Materials Genome Initiative.^{12,13}

Theory-driven experimental synthesis has been particularly fruitful in the field of inorganic nitride materials,¹⁴ which is much less explored compared to other chemistries. In contrast to oxygen, chalcogens, halogens, and even other pnictogens, nitrogen does not tend to form naturally occurring minerals, and hence few early observations of nitride crystal structures were recorded by mineralogists in the first half of the 20th century.¹⁵ The following advances in bulk synthesis methods resulted in a large number of first binary and then ternary nitrides being synthesized.^{16–18} Yet there remained a >10× gap between the number of known nitrides and compounds in other inorganic materials systems, most notably oxides.^{19,20} This was in part due to experimental difficulties with bulk nitride synthesis methods that often rely on hazardous precursors,²¹ extreme pressures,²² oxygen-free environments, and high temperatures. Until recently, the low or uncertain experimental “return on investment (ROI),” resulting from high capital investments in synthesis facilities and unpredictability of synthesis outcomes,

Received: August 31, 2021

Revised: January 5, 2022

Published: February 1, 2022



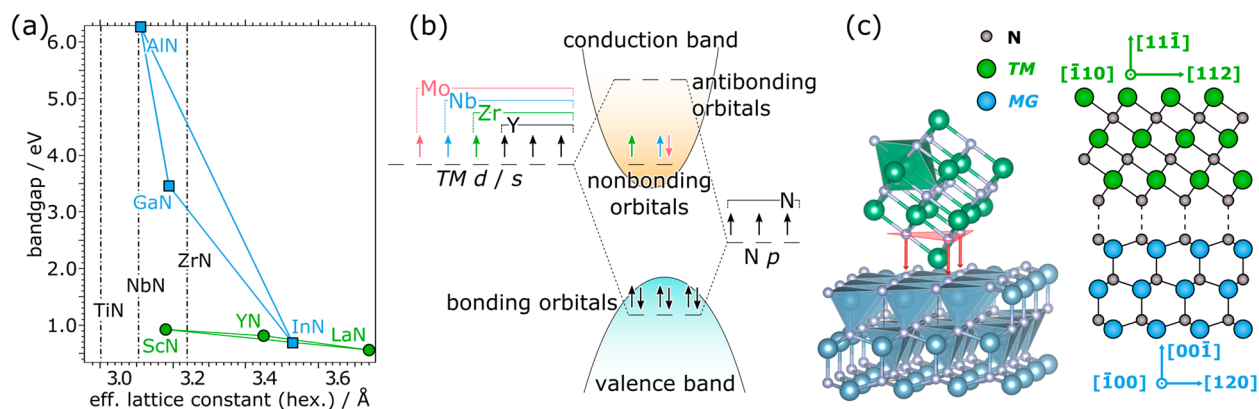


Figure 1. Binary nitride materials. (a) Band gap vs lattice constant for binary nitride semiconductors in wurtzite and rocksalt crystal structures. (b) Schematic of orbital hybridization in transition metal nitride rocksalts showing progressive population of nonbonding states with transition metal group number. (c) Structure schematic showing registration between (001), 4-coordinate wurtzite, and (111), 6-coordinate rocksalt

limited bulk nitride synthesis efforts to a few dedicated laboratories around the world. The modern materials science paradigm has changed these long-standing trends in inorganic nitride chemistry, with experimental syntheses that follow or iterate with theoretical predictions. Numerous examples of experimental synthesis of theoretically predicted materials have been demonstrated,^{23,24} including nitrides studied by our^{25,26} and other groups.^{27,28} Several of these studies on synthesis of nitride materials used thin film deposition methods, which were originally developed for preparing nitride coatings for practical applications and were found to circumvent many of the bulk synthetic challenges.

This article describes our perspective on the progress in experimental synthesis of theoretically predicted multivalent ternary nitride materials. The multivalent ternary nitrides are defined as materials that have an equal number of cations and anions in the formula unit, with nitrogen as an anion in the -3 oxidation state and two metal elements as cations with the total oxidation state that adds up to a multiple of 3. These materials do not necessarily have the equal number or the highest valence state of the cations but often do have relatively simple crystal structures with a close-packed anion sublattice, such as those derived from wurtzite and rocksalt and their distortions, interlayers, or other combinations. In this perspective article, first we present a brief literature review of the multivalent ternary nitride materials that contain alkali earth elements, explaining their structure and bonding on the example of their parent III–N binary nitride compounds. Second, we describe theoretical predictions of the structures and properties of the Zn- and Mg-based multivalent ternary nitrides, including effects of cation ordering. Third, we summarize advances in experimental synthesis and property measurements of these Zn- and Mg-based nitride materials in wurtzite-derived, rocksalt-derived, and mixed layered crystal structures. This perspective on progress with multivalent ternary nitrides should inspire experimental synthesis of other theoretical predicted materials.

2. LITERATURE REVIEW

2.1. Binary Nitride Materials. The prototypical nitride semiconductors are compounds with main group metals, such as the III–N materials and their alloys. These nitride compounds adopt a 4-coordinate wurtzite crystal structure ($3.1 \text{ \AA} \leq a$ lattice parameter $\leq 3.55 \text{ \AA}$) and are typically prepared as epitaxial thin films on each other, (001) sapphire, (111) silicon, and (001)

silicon carbide. The unique position of nitrogen on the periodic table lends a favorable combination of properties to III–N semiconductors. They exhibit direct band gaps at intermediate energy between oxides and other pnictides (Figure 1a), ranging from $\sim 0.7 \text{ eV}$ (InN) to $\sim 3.4 \text{ eV}$ (GaN) to $\sim 6.3 \text{ eV}$ (AlN), lower than corresponding oxides.²⁹ They also have low electron effective masses (e.g., $0.2 m_e$ for GaN),³⁰ with lower propensity to exhibit small polaron charge trapping compared to oxides^{31,32} but better tolerance to defects than other pnictides (e.g., phosphides, arsenides).^{33,19} These properties position III–N semiconductors as technologically relevant materials, such as $\text{In}_x\text{Ga}_{1-x}\text{N}$ light emitters in blue and green LEDs, achieved by varying the band gap with composition control. Similarly, AlN piezoelectrics are the basis for bulk and surface acoustic wave filters used in modern telecommunications,³⁴ and GaN transistors are used in radio frequency electronics and anticipated to replace the Si/SiC standards in intermediate-voltage power electronics applications. These are only a fraction of the uses for III–N semiconductors.³⁵

The other class of widely used binary or alloyed nitride materials are early transition metal nitrides, which are studied as coatings, photonic materials, superconducting materials, and refractory ceramics.³⁶ In contrast to the III–N compounds, these nitride materials adopt a 6-coordinate rocksalt structure. From a bonding perspective shown in Figure 1b, three of the transition metal d orbitals hybridize with the nitrogen p orbitals creating bonding and antibonding bands, while the residual d states remain nonbonding at intermediate energy. The nitrides-containing group III transition metals (Sc, Y, La) have completely filled bonding states and are thus narrow gap semiconductors, with low-temperature magnetic ordering in the case of lanthanide series metals (Pr, Nd, Gd, Eu, Dy etc.).^{37,38} In the nitrides of group IV transition metals (Ti, Zr, Hf), electrons partially fill the nonbonding states, and the resulting compounds are refractory metals. Moving to group V transition metal nitrides (e.g., NbN), the rocksalt crystal structure is often observed experimentally but becomes less stable relative to other polymorphs since a smaller fraction of electrons are bonding. Once nonbonding states are completely occupied (e.g., in MnN with a defect rocksalt structure)³⁹ and antibonding bands must be filled, the rocksalt structure is altogether destabilized, for example, in zincblende FeN^{40} or CoN^{41} . Close-packed planes perpendicular to the [111] lattice vector of the 6-coordinate rocksalt structure exhibit hexagonal symmetry similar to that of

[001] in 4-coordinate wurtzite structure. Thus, coherent interfaces between early transition metal nitrides and main group III Ns can be achieved in these crystallographic orientations, as shown in Figure 1c by a schematic made using VESTA.⁴²

There is also a family of nitrogen-rich binary transition metal nitrides with metals in their highest oxidation states and unequal cation/anion stoichiometry, such as Zr_3N_4 ,⁴³ Hf_3N_4 ,⁴⁴ Ta_3N_5 ,⁴⁵ and MoN_2 .⁴⁶ These are semiconductors based on orthorhombic crystal structures with 6-coordinate metal polyhedra. Some of these phases have been studied as photoanodes for water splitting applications. The most studied example, Ta_3N_5 , has been integrated into tandem cells with >7% solar-to-hydrogen conversion efficiency.⁴⁷ It is usually prepared by high pressure ammonolysis of metal or compound precursors⁴⁸ but can also be made by more delicate methods such as metathesis⁴⁹ and from vapor.⁵⁰ Examples of such high-valent nitrides persist up to the group VI transition metals, for example, layered Mo_3N_6 (i.e., MoN_2), which is a promising hydrogenation catalyst.⁴⁶ Despite these several examples, it remains difficult to make nitrogen-rich transition metal nitrides due to the relatively weak oxidizing power of nitrogen, but the technological interest has led to new compound predictions awaiting novel synthesis strategies. For example, a nitrogen rich cerium nitride Ce_3N_4 has been predicted as a slightly metastable nitride based on a computational search⁵¹ and remains to be synthesized.

2.2. Multivalent Ternary Nitrides. An alternative approach to realizing new nitride semiconductors discussed here is in ternary chemical spaces, with two metal atoms of different valence states. Over the last few decades several of these multivalent ternary nitrides (see definition above) have been studied both for their novel crystal chemistries and their potential as functional materials. A large subset of these compounds has the general chemical formula ABN_2 , but other stoichiometries with an equal cation/anion ratio such as A_2BN_3 and A_3BN_4 have been also reported. The electronic and crystal structures of these materials can be rationalized starting from binary III–N semiconductors. In contrast to III–N semiconductor alloys made by isovalent substitutions (such as $In_xGa_{1-x}N$), the cation valence is split by replacing the III^{3+} cation with equal quantities of $A^{2+}:B^{4+} = 1:1$ cations in ABN_2 ^{52–54} or $A^{2+}:B^{5+}=2:1$ in A_2BN_3 ²⁶ and $A^{2+}:B^{6+}=3:1$ in A_3BN_4 ,⁵⁵ all of which have equal cation/anion stoichiometry and preserve the nominal charge balance with N^{3-} anions and semiconducting behavior.⁵⁶ It is also possible to replace the III^{3+} cation with different ratios of transition metal cations that can change the oxidation state, such as in $Sc^{3+}Ta^{3+}N_2$ ⁵⁷ or $Mg^{2+}Ta^{3.5}N_3$,⁵⁸ likely resulting in metallic behavior. The prototypical binary $III^{3+}-N^{3-}$ semiconductors are GaN and ScN that adopt wurtzite and rocksalt structures, respectively, and similarly down the III^{3+} main group ($MG = Al, Ga, In$) and transition metal ($TM = Sc, Y, La$) columns of the periodic table (Figure 1a).^{35,36} The corresponding multivalent ternary nitrides of these two parent binary categories can be separated into four types of cation mutation. For example, in the case of ABN_2 shown in Figure 2a, these are $AE^{2+}TM^{4+}$, $AE^{2+}MG^{4+}$, $Zn^{2+}TM^{4+}$, and $Zn^{2+}MG^{4+}$, where $AE = Mg, Ca, Sr, Ba$ alkaline earth, $MG = Si, Ge, Sn$, and $TM = Ti, Zr, Hf$. The Cd and Hg candidates that are below Zn on the periodic table are not included in Figure 2a, because ABN_2 compounds containing these elements have not been experimentally realized and only computational predictions exist.⁵⁹

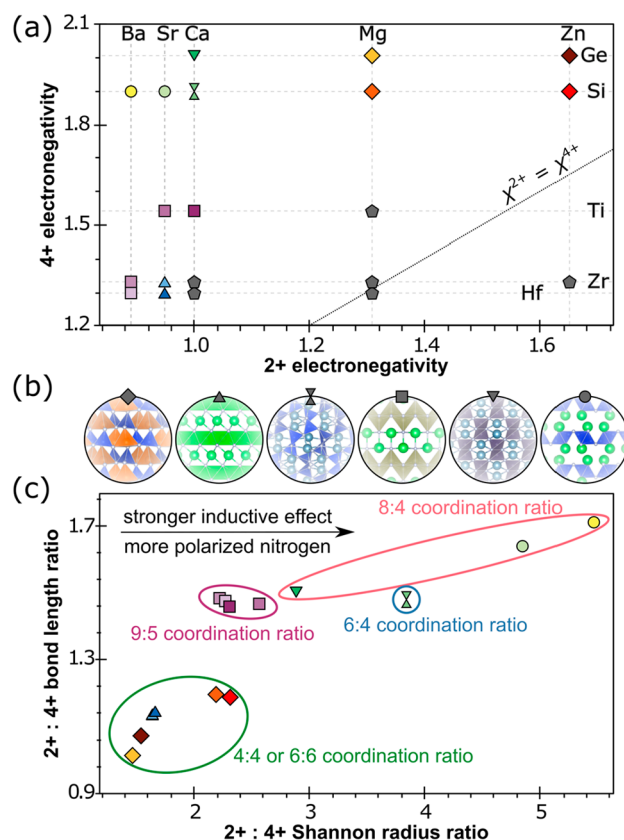


Figure 2. Multivalent ternary nitrides. (a) Electronegativity χ of the A^{2+} and B^{4+} metal ions in various $A^{2+}B^{4+}N_2$ compounds. Points farther from the $\chi^{2+} = \chi^{4+}$ line tend to have more anisotropic structures. Gray pentagon markers have not been synthesized in cation-ordered form. (b) Schematics showing the structure families found in ABN_2 compounds. (c) Cation-ordered compounds from (a) plotted as a function of reported bond length ratio and constituent ion Shannon radii ratio r^{2+}/r^{4+} . Marker shapes and colors are consistent across all panels. Gray pentagons indicate materials that have been reported experimentally but not with an ordered cation sublattice.

Because the differences in cation size (r)⁶⁰ and electronegativity (χ)⁶¹ vary widely across these four categories and because nitrogen is a polarizable anion,⁶² the bonding and structures of multivalent ternary nitrides can be diverse.⁶³ In cases with extreme differences in metal ion size or electronegativity, exotic structures are observed (Figure 2b). For example, in $AEMGN_2$ where $AE = Ba$ or Sr and $MG = Si$, nitrogen localizes around silicon forming edge-sharing pairs of SiN_4 tetrahedra surrounded at much greater distances by 8-coordinate AE atoms⁶⁴ (circle plot markers in Figure 2). This is due to a strong inductive effect,⁶⁵ whereby the electropositive AE atoms readily donate charge, facilitating directional covalent interactions between Si and N.²⁵ As differences in metal ion size or electronegativity decrease, for example, by replacing Ba or Sr with smaller and more electronegative Ca, the nitrogen becomes slightly less polarized, forming corner-sharing tetrahedra around 6-coordinate Ca (hourglass plot markers in Figure 2). For cases where differences in cation size and electronegativity are small (e.g., $MgSiN_2$ ⁶⁶ or $SrZrN_2$,⁶⁷ respectively, shown by diamond and up pointing triangle plot markers in Figure 2), structural analogues to wurtzite and rocksalt are observed, with reduced symmetry from cation site ordering, which is sometimes referred to as “coloring”.⁶⁸ Even within a single structural family (e.g.,

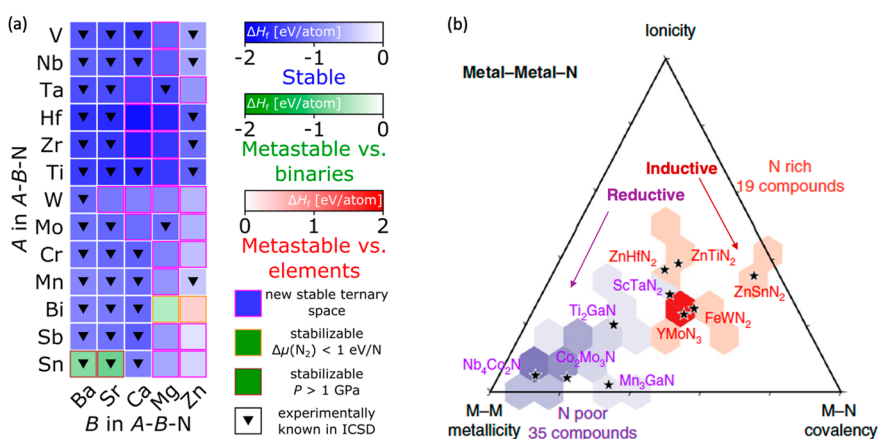


Figure 3. Theoretical ternary metal nitride stability map. (a) Broad-scale computational stability trends in ternary inorganic nitrides $A-B-N$, showing stable and metastable clusters of materials, highlighting stability analysis of parts of ternary $Mg-M-N$ and $Zn-M-N$ material classes. (b) Metallicity, ionicity, and covalency of selected stable ternary nitrides, hexagonally binned and colored by nitrogen excess or deficiency of the ternary compared to the binaries, with color intensity corresponding to the number of materials. Adapted with permission from ref 25. Copyright 2019 Springer Nature.

rocksalt-derived $MgTiN_2$ vs $MgZrN_2$), different coloring motifs are expected with changes to the relative polarizing power of metal ions,⁶⁹ similar to trends observed in oxides.⁷⁰ Despite these structural variations, in each case the *TM* ions often tend to have a *d0* electron configuration suitable for semiconductor applications, and finite band gaps in the range of 1–2 eV have been calculated by GW. Interestingly, Ce atoms can serve in either a smaller 4+ cation role as in $SrCeN_2$ or $CaCeN_2$ with rocksalt-derived structures⁷¹ or in a larger 3+ cation role separating $Mn-N$ planes in the Ce_2MnN_3 multivalent nitride.⁷²

Historically, most of the experimental work on multivalent ternary nitrides has involved bulk synthesis and characterization approaches. Many such preparations have employed a conventional solid-state reaction from binary nitride^{67,73–75} or metal⁷⁶ precursors, though other approaches such as synthesis using supercritical ammonia^{77,78} and Na-flux synthesis using sodium azide as a nitrogen source have also been employed.⁷⁹ Bulk synthesis of such compounds often leads to materials with precise ordering on the cation sites. In contrast to the high temperatures and/or pressures used by bulk synthesis, thin film preparations tend to proceed at low pressure and intermediate temperature, for example, during MBE,⁸⁰ sputtering,⁸¹ and MOVPE.⁵³ These approaches often result in materials with mixed occupancy on cation sublattices,⁵³ though calculations show that statistically random cation configurations are unlikely.^{82,83}

One important remaining question about the multivalent ternary nitride materials is related to the cation order/disorder. For example, in the case of ABN_2 , many of the materials that have been made as thin films are also close to the line where $\chi^{2+} = \chi^{4+}$ and $r^{2+}/r^{4+} = 1$, making it unclear if the propensity for mixed occupancy on cation sublattices is related to the cation-matched electronegativities, ionic radii, or thin film synthesis methods. On one hand the more radius-matched but less electronegativity-matched $ZnGeN_2$ can be made in a cation-ordered configuration by both film and bulk methods.^{78,84} On the other hand there are no conclusive reports on the more electronegativity-matched but less radius-matched $ZnSnN_2$ and $MgSnN_2$ in a cation-ordered (enthalpically favored) configuration by either bulk^{85,86} or film^{87,88} methods. Thus, it appears that the elemental properties (electronegativities, radii) play a more important role than synthesis methods (bulk, film), but this question requires further study. In addition to these order/

disorder questions, several multivalent ternary nitride compounds are still missing from databases or literature. For example, the most striking gap in the family of ABN_2 materials is that no compounds have been reported containing both Zn^{2+} and TM^{4+} until this year.⁸⁹ Experimental reports of $CaZrN_2$ and $CaHfN_2$ also do not exist, which is surprising given their predicted chemical and structural similarity to the analogous Sr-containing compounds.⁹⁰ Experimental information is also absent for the $(Sr, Ba)GeN_2$ material space despite the experimental existence of the related $MgGeN_2$ compound. Whether these materials are less explored due to chemical instability, difficulty of synthesis, lack of interest, or for other reasons is not immediately clear. These “missing” but chemically plausible multivalent ternary materials have led to several computational surveys to broadly determine and map the stability of novel nitrides, as discussed next.

3. COMPUTATIONAL PREDICTIONS

A map of the inorganic ternary metal nitrides²⁵ has been created based on data-mined structure predictions (DMSP)⁹¹ and DFT stability calculations, an approach that was used in the past to predict binary nitrides⁹² and benchmarked against more accurate SCAN calculations.⁹³ As a result of this study, more than 200 new stable ternary nitride compounds across nearly 100 ternary $A-B-N$ chemical spaces have been predicted (Figure 3a), approximately doubling the number of previously reported ternary nitride materials. Clustering of this data set using a machine learning algorithm and analyzing it in terms of chemical bonding revealed several interesting large-scale stability trends in ternary nitride materials (Figure 3b). One example is a new “reductive” stabilization mechanism in some ternary nitrides, in contrast to the known “inductive” stabilization mechanism for alkali-metal-containing ternary nitrides where electron transfer from metal to nitrogen is stronger in the presence of an alkali element.^{94,65} This “reductive” effect in metal–metal nitrides leads to weaker electron transfer to nitrogen (i.e., nitrogen is reduced) in the ternary compared to constituent binary nitrides, because of stronger metal–metal bonding compared to metal–nitrogen bonding. Despite the demonstrated power of DMSP and DFT for predicting new families of ternary nitrides and identifying new chemical mechanisms, more computationally expensive

Table 1. Summary of Calculated Thermodynamic Stability and Electronic Structure Properties of Multivalent Ternary Zn–*TM*–N and Mg–*TM*–N Materials in Their Cation-Ordered Thermodynamically Stable Form^a

material formula	parent structure	space group	ΔH_f (eV/atom)	ΔH_D (eV/atom)	electronic E_g^{el} (eV)	direct E_g^{dir} (eV)	electron m_e^*/m_0	hole m_h^*/m_0
ZnTiN ₂	wurtzite	33	−0.87	−0.05	3.35	3.77	2.10	5.57
ZnZrN ₂	wurtsalt	156	−1.10	−0.05	3.14	3.82	6.64	1.51
ZnHfN ₂	wurtsalt	156	−1.20	−0.07	3.38	3.81	5.39	1.51
Zn ₂ NbN ₃	wurtzite	36	−0.52	−0.08	3.57	3.63	1.08	4.39
Zn ₂ TaN ₃	wurtzite	36	−0.63	−0.16	3.80	3.87	1.32	3.66
Zn ₃ MoN ₄	wurtzite	31	−0.22	−0.08	3.94	4.10	6.24	2.06
Zn ₃ WN ₄	wurtzite	31	−0.28	−0.19	3.96	4.20	1.21	1.93
Zn ₂ SbN ₃	wurtzite	36			1.71	1.71	0.37	2.46
MgTiN ₂	rocksalt	13	−1.42	−0.20	0.91	0.92	1.44	1.43
MgZrN ₂	rocksalt	141	−1.62	−0.16	1.47	1.47	0.63	1.61
MgHfN ₂	rocksalt	141	−1.72	−0.18	1.79	1.79	0.63	1.54
Mg ₂ NbN ₃	rocksalt	12	−1.18	−0.20	1.84	2.26	0.62	1.92
Mg ₂ TaN ₃	rocksalt	12	−1.33	−0.31	2.12	2.50	0.58	1.90
Mg ₃ MoN ₄	wurtzite	31	−1.19	−0.20	5.25	5.35	6.44	5.93
Mg ₃ WN ₄	wurtzite	31	−0.92	−0.22	5.17	5.40	1.48	5.61
Mg ₂ SbN ₃	wurtzite	36			3.14	3.14	0.44	2.38

^aOther data for these compounds are available at materials.nrel.gov. The band gaps are predicted using the GW method and effective masses are extracted from GW DOS calculations with an integration depth corresponding to 1000 K.

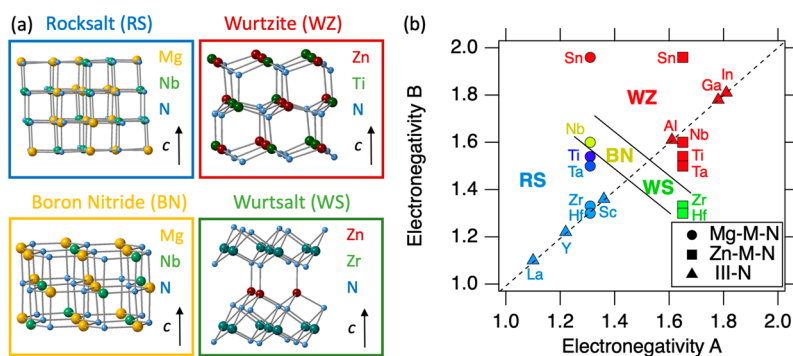


Figure 4. Predicted crystal structures of ternary nitrides. (a) Predicted crystal structure types for Mg–*M*–N and Zn–*M*–N materials, including rocksalt (RS), wurtzite (WZ), boron nitride (BN), and wurtsalt (WS). (b) Clustering of various *A*–*B*–N nitride structures in coordinates of *A* and *B* electronegativities, showing that BN and WS structure appear in intermediate range between more ionic RS compounds and more covalent WZ compounds, with the color legend the same as in (a) and light vs dark blue indicating different cation ordering.

calculations are needed to verify the predicted crystal structures, especially for materials that contain first row (3*d*) magnetic transition metal ions. Thus, below we describe more detailed computational predictions for Zn–*M*–N and Mg–*M*–N families of materials where *M* is a metallic element and analyze their calculated crystal structure, electronic properties, and propensity to cation disorder. One of the reasons that these Zn-based and Mg-based material systems are interesting is that they are much less explored compared to the chemically related Sr–*M*–N and Ba–*M*–N compounds reviewed above.^{63,79}

3.1. Structure and Stability. In the large-scale surveys of nitride materials,^{25,27,95} structure prototyping approaches^{23,91,96} are often used to perform a high throughput screening for the potential stability of candidate materials. These approaches are computationally efficient because they rely on already known crystal structures archived in databases like the Inorganic Crystal Structure Database (ICSD).¹ For a given candidate chemical composition, the total number of structures with suitable stoichiometry can be further down-selected via various data mining strategies, including the DMSP mentioned above and related approaches.^{91,97,98} Such prototyping approaches are appropriate for predicting the existence of compounds at new compositions because even if the ground state structure is not

identified, the prediction can still point to a new chemical space containing compounds that can be experimentally synthesized, as long as a polymorph with negative formation enthalpy relative to any competing decomposition reactions is found. However, for chemical compositions like nitrides with smaller existing data for selection of potential structures and algorithm training compared to, e.g., oxides, the structure prototyping approach becomes less reliable. This is a problem because electronic structure properties often depend very sensitively on the crystal structure. Therefore, it is important to determine the crystal structure to a high degree of confidence for materials whose existence and synthesizability have been inferred from a broad search with less stringent structure selection.

Unconstrained structure prediction algorithms avoid the limitations of structure prototyping by generating new structures and down-selecting by energy minimization criteria. A range of different unconstrained structure prediction approaches exist, including evolutionary algorithms,^{99,100} particle swarm optimization,¹⁰¹ random structure search,¹⁰² and basin hopping.^{103,104} Our Kinetically Limited Minimization (KLM) approach⁵¹ combines elements of random sampling and basin hopping: it generates a large number of seed structures (typically ~100) based upon random lattice vectors, with mild constraints

on the cell shape, and random atomic initial coordinates in the cell. It then optimizes the individual seed structures by sequential displacement of a randomly chosen atom and accepts the structure if the energy is lowered. The resulting structures are relatively deep local minima, and the method is well suited to identify stable polymorphs. An essential feature of our implementation is the enforcement of judiciously chosen pairwise minimal distances between the different atom types both after random seed generation and after each displacement step. This feature dramatically reduces the size of the configuration space, thereby increasing the success rate, which can be defined as the number of ground state discoveries divided by number of seed structures. It also helps to maintain a remarkably size-independent success rate⁵¹ despite the nominal exponential scaling of the number of local minima.

Following the study of inorganic ternary metal nitride materials using DMSP (Figure 3),²⁵ an unconstrained structure prediction was performed for a subset of the full search space, i.e., for the Zn–*M* and Mg–*M* nitrides (*M* = Ti, Zr, Hf, Nb, Ta, Mo, W, Sb), using the KLM algorithm.⁵¹ Theoretical predictions for the crystal structure and thermochemical stability of all these materials in materials.nrel.gov¹⁰⁵ are presented in Table 1. In about 70% of the cases, KLM was able to identify a lower energy structure, but in most cases the DSMP energies were still within 0.1 eV/atom. For the Zn–*M*–N materials KLM predicts wurtzite-derived crystal structures with various cation ordering (Figure 4a) for transition metals *TM* = Ti, Nb, Ta, W, Mo, as well as *M* = Mo,⁵⁵ Sb. These wurtzite-derived Zn–*TM*–N compounds are structurally and chemically related to main group II–IV–N₂ materials, which have received significant computational attention in the past two decades.^{106,107} Another layered crystal structure that consists of alternating wurtzite and rocksalt layers (Figure 4a) was predicted for Zn–*TM*–N with *TM* = Zr and Hf, consistent with literature reports using structure prototyping¹⁰⁸ and an evolutionary algorithm.²⁷ We refer to this layered structure as “wurtsalt” (WS),⁸⁹ a portmanteau of wurtzite and rocksalt, because of the alternating 4-fold and 6-fold coordination environment between its layers. For the Mg–*TM*–N (*TM* = Ti, Zr, Hf, Nb) materials,²⁶ theoretical predictions using the KLM algorithm indicate rocksalt-derived structures with various cation ordering (Figure 4a), including motifs in the layered α -NaFeO₂ structure with space group (SG) 166 for MgTiN₂ and the γ -LiFeO₂ structure (SG 141) for both MgZrN₂ and MgHfN₂,^{109,110} consistent with other computational studies of MgTiN₂,⁶⁹ and MgTMN₂ (*TM* = Ti, Zr, Hf).²⁶ A close energy competition exists for Mg₂NbN₃ and Mg₂TaN₃ between 6-fold coordinated rocksalt-derived structure (SG 12) and 3/5-fold coordinated layered structure related to hexagonal boron nitride (BN-type, SG 15) (Figure 4a). On the other hand, Mg-based ternary nitrides with group VI transition metals (e.g., Mo, W) and main group metals (e.g., Sb, Sn) were predicted to form in WZ-derived structures (Figure 4a), such as for Mg₂SbN₃¹¹¹ and MgSnN₂.⁸⁸

It is notable that many members of the Zn–*M*–N and Mg–*M*–N families mentioned above assume wurtzite- and rocksalt-derived structures, where the ground state is distinguished by a certain ordering pattern of the cations. Thus, the unconstrained structure search can be augmented by an analogous on-lattice search for these likely parent lattices, using initial random atomic decorations and atomic swapping instead of displacement.⁵¹ This approach better scales to larger system sizes than the unconstrained search and bridges structure prediction with alloy

theory, where a cluster-expansion^{112,113} and model Hamiltonians are typically used to enable simulation of system sizes above 1000 atoms with statistics suitable for finite-temperature thermodynamic studies.^{114,115} Such a cluster expansion approach was also employed in a Monte Carlo study on nonequilibrium disorder in the ZnGeN₂ ternary nitride.¹¹⁶ In the rocksalt-derived Mg–*TM*–N systems, Monte Carlo simulations in smaller 64 atom cells were performed directly on DFT energies, to validate the predictions of the KLM methods and to obtain insight on the impact of cation disorder on the electronic structure properties,²⁶ as discussed below.

3.2. Structural and Chemical Trends. Three out of the four predicted crystal structures in Figure 4a (RS, WZ, BN) are well-known for other compounds. The 6-fold coordinated RS structure is formed by two cations filling octahedral sites in a face-centered cubic (FCC) nitrogen sublattice (also known as cubic closed packed, CCP) and is similar to ScN, YN, and LaN binary nitride structures.³⁶ The 4-fold coordinated WZ structure is formed by two cations filling tetrahedral sites in a hexagonal closed packed (HCP) nitrogen sublattice and is the same as for AlN, GaN, and InN binary nitride structures.¹¹⁷ The layered BN structure has three shorter bonds in M–N planes (similar to graphite) and two longer bonds out of M–N planes (similar to h-BN), with an HCP nitrogen sublattice.¹¹⁸ The fourth, less-well-known, WS structure (Figure 4a) also features an HCP nitrogen sublattice, with the *TM* cation (e.g., Zr, Hf) filling 6-fold coordinated sites in distorted octahedral coordination (similar to RS) and the other cation (i.e., Zn) filling 4-fold coordinated sites in distorted tetrahedral coordination (similar to WZ), with CuScS₂ as a prototype.^{119,120}

The four distinct predicted crystal structure types (WZ, BN, RS, WS) have four different atom coordination environments (4-fold; 3- or 5-fold; 6-fold; mixed 4- and 6-fold, respectively), but they are not unrelated to each other. The BN and WZ can be viewed as linear distortions of one another, where BN-type structure can be obtained by flattening of metal–nitrogen planes in WZ-type structure.^{121,122} This flattening is also the first step along the transition pathway from WZ to RS, followed by compression in an orthogonal direction.^{123,124} The exact transition pathway to and from the WS structure, as well as its energetics, is presently not clear. However, it may be related to the pressure-induced phase transition in AgAlS₂ from zincblende (ZB) related tetragonal chalcopyrite structure to trigonal ilmenite (IL) related structure¹²⁵ that differs from WS structure by distortion in tetrahedra. It is also interesting to note that the layered WS structure is related to 2D materials. Removing tetrahedrally coordinated cations from the wurtsalt (WS) structure of ZnZrN₂ would result in hypothetical ZrN₂ with octahedrally-coordinated three atom thick layers, typical of TiS₂,¹²⁶ SnS₂,¹²⁷ and TaS₂.¹²⁸ Similarly, removing Td-coordinated cations from the “wurtzeline” (WL, a portmanteau of wurtzite + nickeline) structure of ZnMoN₂ (related to AgNbS₂)^{129,130} would result in three atom thick layers of trigonal prismatic MoN₂⁴⁶ with MoS₂-type structure.^{131,132} These 2D chalcogenide structures are now widely studied as “emerging materials”^{133,134} and were known in the past as “intercalation compounds”.¹³⁵

Next, we analyze the chemical trends in crystal structure of Zn–*M*–N and Mg–*M*–N focusing on the overarching coordination preferences rather than specific crystallographic symmetries and cation sublattice ordering. Computationally predicted crystal structures and thermodynamic stability of Zn- and Mg-based ternary metal nitrides, containing selected

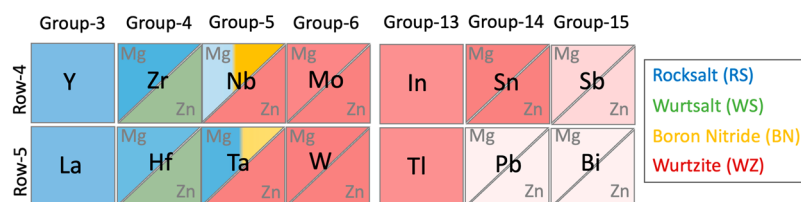


Figure 5. Periodic table trends of structure and stability in ternary nitrides. Trends in structure (color) and stability (darker vs lighter shade) as a function of M in $Mg-M-N$ and $Zn-M-N$, showing diversity of structures for early transition metals and decreased stability for main group elements. The underlying computational data for this analysis from materials.nrel.gov are summarized in Table 1.

second-row and third-row transition metal (TM) and main group (MG) elements, are summarized in Figure 5 and listed in Table 1 based on data from materials.nrel.gov. Both Zn- and Mg-containing ternary nitrides that contain MG or group VI TM elements are predicted to crystallize with tetrahedrally bonded wurtzite-derived crystal motifs (Figure 5). These nitride compounds are calculated to be thermochemically stable for TM elements and Sn and metastable with respect to decomposition into N_2 for other MG elements (Pb, Sb, Bi). In contrast, predictions for early TM elements differ between Zn-based and Mg-based ternary nitrides (Figure 5). For Zn-based compounds, Zn_2NbN_3 and Zn_2TaN_3 are predicted form with only WZ-derived crystal motifs, but $ZnZrN_2$ and $ZnHfN_2$ are predicted to form in a layered wurtzite crystal structure featuring 4-fold tetrahedrally coordinated Zn atoms and 6-fold octahedrally coordinated Zr or Hf atoms. (Figure 4a). For Mg-based compounds, $MgZrN_2$ and $MgHfN_2$ are calculated to form with octahedral, RS-derived crystal motifs, whereas competition between RS and layered crystal structures (Figure 4a) similar to boron nitride (BN-like) is predicted for Mg_2NbN_3 and Mg_2TaN_3 . Other $Mg-M-N$ have been reported in the literature with intermediate oxidation states and layered crystal structures, such as $MgTa_2N_3$ ⁵⁸ and $MgMoN_2$ ¹³⁶ with “rocksalt” (RL) crystal structure comprised of alternating layers of octahedral rocksalt-like and trigonal prismatic nickeline-like coordination environments.

Analysis of the chemical trends in crystal structure of Zn- and Mg-based ternary metal nitrides is displayed in Figure 4b, showing their “structure map” in coordinates of electronegativity (χ) of the two metals A (Zn or Mg) and B (TM or MG element) in a ternary compound, in comparison with binary III–N compounds that fall along the $\chi_A = \chi_B$ line. For larger χ the WZ structure is formed, and for smaller χ the RS structure is preferred. The specific cation ordering within RS structure depends on the electronegativity difference, where a small difference leads to 3D-dispersed $LiFeO_2$ -type RS structures, and a large difference leads to 2D layered $\alpha-NaFeO_2$ -type RS structures or even a 2D layered $KCoO_2$ -type structure where related A = Ba, Sr atoms are 5-fold coordinated.⁶³ When both χ values are in the 1.4–1.6 range, then the WS structure is formed if $\chi_A > \chi_B$ and BN-type structure is formed if $\chi_A < \chi_B$. Thus, it appears that the structure preferences for these Zn- and Mg-based nitrides are determined by the electronegativity χ of A and B elements (Figure 4b), and elemental radii r of A and B cannot explain these structural trends. This seems to be the case not only for ternaries but also for simple binaries (Figure S1a), where well-known Pauling rules^{61,137} and similar factors^{138,139} have been extensively used for clustering in the past. However, average radii r can be used together with average electronegativity χ to provide a reasonable diagrammatic separation (Figure S1b). Overall, this observation on the importance of

electronegativity compared to elemental radii in determining the crystal structure supports the idea of complex ionic/covalent bonding ternary metal nitrides with charge transfer between metals.²⁵

3.3. Electronic Properties. Electronic properties, such as direct and indirect band gaps as well as hole and electron effective masses, have been systematically predicted for a wide range of $Zn-M-N$ materials in literature.²⁷ For the multivalent ternary $Zn-TM-N$ with $TM = Ti, Nb, Ta, W, Zr, Hf$, the calculated band gaps are all in the 3–4 eV range, quite similar to that of GaN, though some of them are slightly (0.1–0.3 eV) indirect. These predicted band gaps at the HSE level of theory are wider than earlier theoretical study of $TM = Ti, Zr, Hf$ candidates at the GGA level of theory which also predicted their piezoelectric properties.¹⁰⁸ The calculated $E(k)$ electron and hole effective masses reported in literature for the $Zn-TM-N$ ($TM = Nb, Ta, W$) with wurtzite-derived structure are more balanced (0.5–1.0 m_0 for both) compared to GaN ($m_e^* = 0.2m_0$ vs $m_h^* = 2.0m_0$) and are inverted for the $Zn-TM-N$ ($TM = Zr, Hf$) with layered wurtzite structure featuring light holes and heavy electrons. Theoretical predictions of average isotropic effective masses at the GW level of theory for all these materials in materials.nrel.gov¹⁰⁵ summarized in Table 1 are qualitatively consistent with these earlier theoretical studies. However, these average isotropic effective masses extracted from the GW DOS with an integration depth corresponding to 1000 K are larger than the tensorial anisotropic effective masses extracted from HSE $E(k)$ calculations, which are much more computationally expensive at the GW level of theory. Thus, these serve as upper limits of the actual effective mass value.

Our predictions of the electronic properties of multivalent ternary $Mg-TM-N$ materials with $TM = Ti, Zr, Hf, Nb$ that tend to crystallize in rocksalt-derived structures²⁶ are quite different compared to the wurtzite-derived or layered $Zn-TM-N$ compounds (Table 1). For $Mg-TM-N$, the electronic band gaps are generally lower (1–2 eV) and more indirect (~ 1 eV), while the DOS effective masses are also lower and well-matched between holes and electrons (0.5–1.5 m_0 for both). Another distinguishing feature of these rocksalt-derived ternary nitrides is the large static dielectric constant (25–75 ϵ_0) compared to the wurtzite-derived ternary nitrides (5–10 ϵ_0) due to their much stronger ionic component. The $Mg-TM-N$ ($TM = Ti, Zr, Hf$) GW band gap calculation results²⁶ are consistent with an HSE study that also calculated their mechanical properties¹⁴⁰ and wider than earlier theoretical studies at the GGA level of theory that also predicted their thermoelectric properties⁶⁹ and calculated some defect formation energies.¹¹⁰ For Mg_2SbN_3 that crystallizes in a wurtzite-derived rather than rocksalt-derived crystal structure, the band gap is much wider (>3 eV) and direct.¹¹¹ Even wider (>5 eV) but slightly indirect (0.1–0.2

Table 2. Calculated Formation Enthalpies (ΔH_f) and Polymorph Energies (ΔH_p), for Crystal Structures of Stable and Metastable Mg–M–N and Zn–M–N, As Well As Their Electronic Properties^a

material formula	ΔH_f (eV/atom)	ΔH_p (eV/atom)	space group	struct. type	E_g^{el} (eV)	E_g^{dir} (eV)	m_e^* (m_0)	m_h^* (m_0)
MgZrN ₂	-1.62	0.000	141	rocksalt	0.94	0.94	0.7	1.9
MgHfN ₂	-1.73	0.000	141	rocksalt	1.30	1.30	0.6	1.8
MgTiN ₂	-1.42	0.000	13	rocksalt	0.64	0.64	1.6	1.7
Mg ₂ NbN ₃	-1.18	0.004	12	rocksalt	0.94	1.29	0.7	2.3
Mg ₂ TaN ₃	-1.33	0.000	12	rocksalt	1.39	1.70	0.7	2.4
ZnZrN ₂	-1.03	0.069	141	rocksalt	0.69	1.30	0.5	2.0
ZnHfN ₂	-1.14	0.058	141	rocksalt	0.80	1.49	0.5	2.0
ZnTiN ₂	-0.78	0.090	13	rocksalt	0.83	1.24	2.4	2.4
Zn ₂ NbN ₃	-0.32	0.197	12	rocksalt	0.81	0.81	1.3	1.3
Zn ₂ TaN ₃	-0.46	0.167	12	rocksalt	1.26	1.26	1.2	1.2
ZnZrN ₂	-1.03	0.090	33	wurtzite	2.40	2.90	0.7	8.3
ZnHfN ₂	-1.11	0.100	33	wurtzite	2.23	2.66	0.5	8.9
ZnTiN ₂	-0.87	0.000	33	wurtzite	2.41	2.75	2.7	6.5
Zn ₂ NbN ₃	-0.52	0.000	36	wurtzite	1.98	2.01	1.1	4.2
Zn ₂ TaN ₃	-0.63	0.000	36	wurtzite	2.27	2.49	0.8	3.7
MgZrN ₂	-1.57	0.054	62	BN-type	1.63	1.69	1.4	0.9
MgHfN ₂	-1.66	0.063	62	BN-type	2.01	2.08	1.4	1.0
MgTiN ₂	-1.37	0.050	62	BN-type	0.98	0.98	1.7	0.7
Mg ₂ NbN ₃	-1.19	0.000	15	BN-type	1.44	2.10	1.7	0.9
Mg ₂ TaN ₃	-1.31	0.020	15	BN-type	1.857	2.56	1.6	1.0

^aElectronic (E_g^{el}) and Direct (E_g^{dir}) Band Gaps and Electron (m_e^*) and Hole (m_h^*) Effective Masses, Calculated at the DFT Level and Schematically Illustrated in Figure S6 and Plotted in Figure S2.

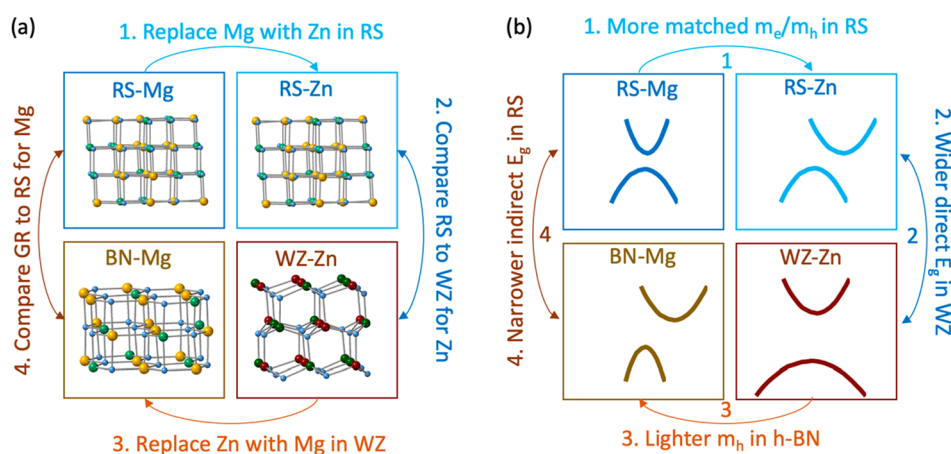


Figure 6. Schematic illustrations of electronic structure trends in ternary nitrides. (a) Crystal structures and (b) band structures for stable RS-type Mg–M–N, metastable RS-type Zn–M–N, stable WZ- or WS-type Zn–M–N, and metastable BN-type Mg–M–N in clockwise order. In both panels, unidirectional arrows represent hypothetical atom replacements, and the bidirectional arrows represent the comparisons between the higher-energy polymorph and the lowest-energy structure, with the numbers corresponding to the order of the discussion in the text.

eV) are the predicted Mg₃MoN₄ and Mg₃WN₄ with wurtzite-derived structures.

Next, we analyze how chemical composition and crystal structure influence electronic structure of Zn- and Mg-based transition metal ternary nitrides, as listed in Table 2 and plotted in Figure S2. To decouple the effects of chemical composition and crystal structure on electronic structure, the calculated properties for thermodynamically stable structures (WZ or WS for Zn-based compounds and BN for Mg-based compounds) are compared to those of hypothetical structures (RS for Zn-based compounds and BN for Mg-based compounds). A graphical illustration of the crystal structure and electronic structure trends is schematically summarized in Figure 6. At a high level, the data in Table 2 and Figure 6 indicate that the structural family (WZ vs WS vs RS vs BN), rather than composition (Zn vs

Mg), is the primary factor which determines the diverse electronic properties calculated for these ternary nitrides. These theoretical results suggest that independent control of structure and composition or the ability to form metastable polymorphs in such compounds is an important step for functional materials design. Note that the presented trends are valid (Figure 6), but the absolute band gaps are likely underestimated (Table 2) as often reported for DFT calculation method, and the density of states effective masses calculated assuming Fermi–Dirac distribution at 1000 K are average compared to anisotropic $E(k)$ effective masses calculated at 0 K. A more systematic description of the composition and structural effects on the electronic properties is provided below in four steps.

First, consider replacing Mg with Zn in the RS-derived crystal structure (Figure 6a), which can be implemented (Zn, Mg)–*TM*–N alloying on underlying RS lattice by thin film growth of the bulk cation exchange method. As Zn replaces Mg, the band gaps remain similar, but direct band gaps convert to slightly indirect band gaps and vice versa (top two blocks in Table 2). With Zn replacing Mg, electron effective masses slightly increase, and hole effective masses remain similar, so together electron and hole effective masses become more matched to each other in RS (Figure 6b).

Second, comparing these electronic structure features of metastable RS-derived to stable WS- or WZ-derived structures for Zn–*TM*–N (Figure 6b), the electron effective masses are similar but hole effective masses are much lower for RS-derived structures. In addition, band gaps significantly decrease for RS compared to WZ or WS (middle two blocks in Table 2). Both lower band gaps and matched electron/hole effective masses are favorable for potential future electronic applications of metastable RS-derived Zn-based transition metal ternary nitrides.

Third, consider replacing Zn with Mg in WZ-derived crystal (Figure 6a), which can be synthetically implemented by, e.g., nucleation from designed amorphous precursors. As Zn is replaced by Mg, the structure instantaneously (dynamically) relaxes from WZ to BN-type, the band gaps decrease slightly compared to Zn-based WZ (bottom two blocks in Table 2), and electron effective masses remain similar while hole masses decrease (by nearly 10× in some cases) to <1 m_0 in BN (Figure 6b).

Fourth, comparing the resulting electronic structure features of metastable BN-type Mg–*TM*–N to stable RS-type Mg–*TM*–N, the band gaps are wider and hole effective masses are actually lower than electron effective masses in BN-type (top and bottom blocks in Table 2). This observation of holes lighter than electrons in metastable BN-type Mg–*TM*–N (Figure 6b) is extremely unusual and potentially interesting for various electronic applications, motivating a search of other compounds that form in this crystal structure or design of heterostructural alloys to tune end-point compounds toward this crystal structure. These theoretical results highlight the importance of independent control of composition and structure in ternary nitrides and other materials.

In summary, from Table 2 and Figure 6 it appears that the crystal structure (e.g., RS vs WZ vs WS vs BN) influences the properties (band gaps, effective masses) more than the chemical composition (i.e., Zn vs Mg). The observation of low hole effective masses in metastable RS-type Zn–*M*–N and metastable BN-type Mg–*M*–N compared to their lowest-energy structures are particularly unexpected and potentially useful for electronic applications. This in contrast to the more gradual and chemically intuitive shift in band gap with Mg/Zn substitution without the change in the structure, where trends can likely be explained by changes in atomic character of the bands using atom-projected density of states (pDOS)¹¹¹ or Crystal Orbital Hamilton Population (COHP)⁵⁵ calculations. In the future, it would be interesting to use these and similar methods^{141,142} to analyze the influence of the structural features (e.g., local coordination, long-range order) on the electronic properties of the materials (band gaps, effective masses), to improve chemical intuition on structure–property relationships in nitrides and other solid state inorganic materials.

3.4. Effect of Cation Ordering. Site disorder on the cation sublattice is an important issue in ternary metal nitrides, as it

influences both the stability of various structures and the resulting properties. For example, changes in band gaps in WZ-derived II–IV–N₂ materials without change in the lattice constant have enjoyed significant attention as a potentially favorable feature for light-emitting diodes and related applications,^{143,53} in contrast to ZB-derived ternary and quaternary chalcogenide photovoltaic absorbers where such disorder is often viewed as unfavorable.^{144,145} Such cation disorder can be modeled using Monte Carlo (MC) simulations, but its high computational cost requires development of a model Hamiltonian, so it has been performed so far only for a few more-studied material systems such as ZnSnN₂^{146,87} and ZnGeN₂^{147,84} discussed below. However, useful insights into the energy cost of cation disorder, as well as the resulting structural distortions and the changes of the electronic structure, can be deduced from the simpler crystal structure prediction calculations in smaller unit cells that are necessarily ordered. To this end, it is useful to analyze not only the lowest-energy ground state structure but also the other energetically low-lying structures produced by the structure search.

Table 3 shows a set of eight Zn and Mg ternary nitrides with predicted wurtzite-derived ground state (gs) crystal structure

Table 3. Comparison of Polytype Properties for Eight WZ-Derived Ternary Nitrides^a

material formula	ground state (gs) space group	lattice Distortion (%)	polytype (pt) space group	polytype energy ΔE_{pt} (meV/cat)	band gap difference ΔE_g (eV)
Zn ₂ SbN ₃	36	0.1	9	9.0	−0.21
Zn ₃ MoN ₄	31	0.1	186	7.1	0.25
ZnSnN ₂	33	0.2	26	1.9	−0.06
Mg ₂ SbN ₃	36	0.5	9	11.5	−0.30
MgSnN ₂	33	0.7	26	10.6	−0.14
Zn ₂ NbN ₃	36	1.5	9	0.9	0.29
ZnGeN ₂	33	2.1	26	53.9	−0.53
MgGeN ₂	33	3.7	26	76.9	−0.79

^aThe first two columns give the orthorhombic space group number of the ordered ground state (gs) and the associated distortion defined as the change in the basal plane lattice parameters relative to ideal WZ. The following columns give the space group number of the lowest energy WZ polytype (pt), as well as its total energy and band gap difference relative to the ground state (gs).

described by an orthorhombic supercell (SG 31, 33, and 36) of the WZ parent lattice (SG 186). Table 3 also shows the space group of the second-lowest energy WZ polytype (pt) found by KLM sampling, along with the total energy and band gap difference with respect to the ground state. In all cases, the ground state and the polytype have the same short-range order configuration as the ground state, e.g., exclusive 2-2 (N–Zn₂Sn₂) motifs in the ABN₂ stoichiometry, exclusive 3-1 motifs in the A₃BN₄ stoichiometry, and a mix of 2-2 and 3-1 motifs in A₂BN₃ stoichiometry. The list in Table 3 is ordered by the distortion of the ideal WZ lattice, defined as the relative change of the *b/a* ratio of the orthorhombic lattice parameters in the basal plane compared to the ideal WZ supercell. The data presented in Table 3 was obtained by performing DFT calculations¹⁴⁸ with the SCAN functional⁹³ on structures obtained in previous sampling efforts.

Table 3 shows that the orthorhombic distortion of the WZ lattice is very small (<0.2%) for Zn₂SbN₃, Zn₃MoN₄, and ZnSnN₂, which should be virtually impossible to identify by the

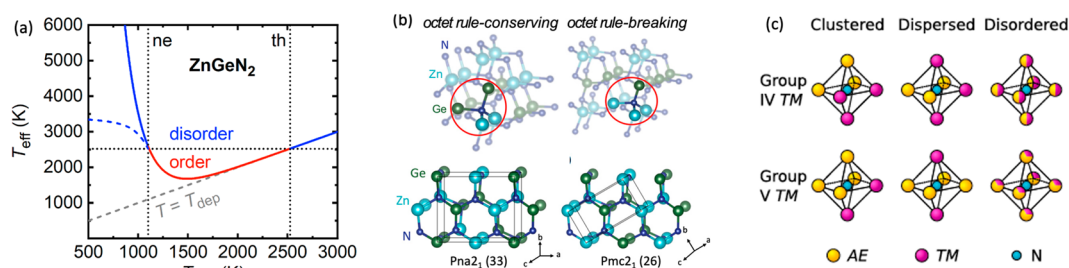


Figure 7. Cation ordering in ZnGeN_2 : (a) Mapping the dependence of T_{eff} , which describes the degree of nonequilibrium disorder, on the deposition temperature T_{dep} for ZnGeN_2 where ne = nonequilibrium and th = thermodynamic. (b) Octet rule-conserving (left) and breaking (right) motifs in wurtzite-derived ZnGeN_2 , with outlined 16-atom ($Pna21$, SG 33) and 8-atom ($Pmc21$, SG 26) orthorhombic primitive cells, respectively. Adapted with permission from ref 116. Copyright 2021 American Physical Society. (c) Clustered, dispersed, and disordered cation coordination motifs of nitrogen atoms in the rocksalt-derived ternary nitrides. Adapted with permission from ref 26. Copyright 2019 National Academy of Sciences.

peak splitting in XRD. A moderate 0.5–0.7% distortion of the ground state in Mg_2SbN_3 and MgSnN_2 correlates with a moderate 10–12 meV/cat polytype energy. On the other hand, ZnGeN_2 and MgGeN_2 with a more substantial distortion (2–4%) also show a much larger ΔE_{pt} energy (50–80 meV/cat). Thus, considering that the polytypes all have the same motif structure as the ground state, it appears that both the distortion and the polytype energy are indicative of the importance of long-range order (LRO) effects. It is noted, however, that Zn_2NbN_3 is somewhat an outlier in this trend, showing a relatively large distortion of 1.5% despite a very small ΔE_{pt} energy. Interestingly, Zn_2NbN_3 also shows other structural anomalies, such as a large deviation from the ideal WZ c/a ratio in a disordered state.⁵⁶

The band gap differences ΔE_g between the polytype and the ground state reasonably correlate with both the distortion and the ΔE_{pt} energy as shown in Table 3. For example, in the case of Zn_2SbN_3 ,¹⁴⁹ the KLM structure sampling identified seven nonequivalent crystal structures in a 12-atom sampling cell within an energy window of 50 meV/cation, exhibiting a clear trend of decreasing band gaps as a function of energy above the ground state.¹⁵⁰ For all the other main group metals in Table 3, the band gap change ΔE_g is negative, indicating that long-range disorder is likely to reduce the gaps by a magnitude that should follow the rough trend of distortion, polytype energy, and gap difference. Interestingly, for the transition metals (Nb, Mo), the band gap change in the polytype structure is positive, making it more difficult to generalize an expectation for other materials. However, it is important to note that the band gap of a system is an intensive property that assumes the minimum (not the average) among the subsystems, and therefore disorder should always reduce the gap. Of course, the very definition of a band gap in a disordered system is somewhat ambiguous, an issue that is being addressed in an ongoing computational study of ZnGeN_2 .¹⁵¹

For a few selected materials presented in Table 3, Monte Carlo (MC) simulations have provided detailed insights into the order–disorder transition. The temperature of these MC simulations can be interpreted as an effective temperature T_{eff} quantifying the degree of disorder resulting from the kinetic limitations that prevent complete cation ordering in nonequilibrium synthesis.¹⁵² At lower deposition temperatures T_{dep} where ionic mobility is strongly limited, T_{eff} can greatly exceed the actual temperature, but the two temperatures eventually converge when full equilibration is established. For example, in ZnGeN_2 (Figure 7a) the thermodynamic (th) order–disorder phase transition is predicted to occur around 2500 K, although a significant degree of nonrandomness remains in the disordered

state. However, this hypothetical thermodynamic order–disorder transition lies outside of the practical pressure range of stability for ZnGeN_2 , which is limited by decomposition driven by the chemical potential reduction of N_2 gas. Instead, according to several experimental observations,¹⁵³ ZnGeN_2 undergoes a nonequilibrium (ne) order–disorder phase transition and loses cation ordering below 1100 K (Figure 7a). The strong increase in T_{eff} with decreasing T_{dep} accounts for the random disorder limit at $T_{\text{eff}} = 400\,000\text{ K}$ ¹¹⁶ in the MC simulation, corresponding to the limit $T_{\text{dep}} = 0\text{ K}$ in this model, where cation ordering is completely suppressed. However, T_{eff} may not reach these high values if the actual temperature controlling the adatom mobility at the surface exceeds the nominal temperature of the substrate (dashed blue line in Figure 7a), e.g., due to the energy imparted by the deposition process (e.g., sputtering).

The ZnGeN_2 and ZnSnN_2 materials studied with MC simulations exhibit interesting differences in the relation between short-range order (SRO) and long-range order (LRO), which is difficult to distinguish by X-ray diffraction. This distinction between SRO and LRO results from non-randomness in the disordered state that can be expected due to electrostatic interactions between heterovalent cations (e.g., Zn^{2+} and Ge^{4+} in ZnGeN_2) in contrast to isovalent alloys (e.g., Al^{3+} and Ga^{3+} in $\text{Al}_x\text{Ga}_{1-x}\text{As}$)¹⁵⁴ without atomic size mismatch.¹⁵⁵ In particular, the energetics of ZnSnN_2 and $(\text{ZnSnN}_2)_{1-x}(\text{ZnO})_{2x}$ alloys are largely determined by SRO effects alone, leading to perfect short-range order (PSRO) configurations that include exclusively ground state motifs, even in the presence of long-range disorder. For example, in pure ZnSnN_2 the MC simulations at effective temperatures below the order–disorder phase transition resulted in PSRO structures that feature only the N– Zn_2Sn_2 motifs (Figure 7b)⁸³ and can also be constructed by sequential stacking of cation rows in the basal planes.⁸² As another example, in the $(\text{ZnSnN}_2)_{1-x}(\text{ZnO})_{2x}$ alloys, the large configurational entropy of these PSRO structures that contains exclusively N– Zn_2Sn_2 and O– Zn_4 motifs at the $x = 0.25$ “magic composition”¹⁵⁶ is sufficient to stabilize the PSRO phase within a temperature window between the phase separated ($\text{ZnSnN}_2 + \text{ZnO}$) and random alloy phases. In contrast to ZnSnN_2 , the LRO and SRO in ZnGeN_2 are strongly coupled,¹¹⁶ so the disappearance of the long-range structural distortions is accompanied by the introduction of the octet-rule breaking motifs (Figure 7b).

The influence of cation disorder on the electronic structure can also be determined from these MC simulations. In general, it appears that the PSRO structures stand out in their ability to

retain ideal delocalized states at both the valence and conduction band edges despite the long-range disorder,^{83,156} but the results vary outside of these PSRO structures. For example, ZnSnN₂ ($E_g = 1.4$ eV)¹⁵⁷ shows a substantial band gap reduction with increasing degree of short-range disorder,⁸³ but the density of states remains continuous and exhibits only moderate localization effects in the valence band. However, in ZnGeN₂ with a much wider gap (3.6 eV) and less dielectric screening,¹¹⁶ the disorder leads to a more pronounced defect behavior and stronger localization effects. In contrast to both of these wurtzite-derived materials, the rocksalt-derived Mg–TM–N with fully oxidized transition metals shows a remarkable tolerance of the electronic and optical properties to disorder,²⁶ which is likely a consequence of the high dielectric constant associated with d^0 transition metals in the rocksalt structure.¹⁵⁸ Another related factor is that Mg–TM–N with RS-derived structure can assume two (clustered or dispersed) locally charge-neutral cation coordination motifs around the nitrogen site (Figure 7c),²⁶ similar to other alkali earth ternary nitrides⁹⁰ and in contrast to tetrahedral systems with only one charge-neutral motif (Figure 7b).⁵³

4. EXPERIMENTAL SYNTHESIS

To validate computational predictions in the map of the inorganic ternary nitrides²⁵ and discover new nitride materials beyond this map, we synthesized many new ternary metal nitride materials using cosputtering from metal targets in nitrogen gas, as summarized in Table 4. For several of these Zn- and Mg-based multivalent ternary nitrides, crystal structures determined from

Table 4. Ternary Metal Nitrides Synthesized at NREL in the Past 5 Years, in Film and Bulk Form^a

chemical composition	structure prototype	absorption onset (eV)	resistivity (ohm cm)	sample form	ref
MgTiN ₂	rocksalt	2.0	3×10^4	film	26
MgZrN ₂	rocksalt	1.8	6×10^2	film	160
				bulk	159
MgHfN ₂	rocksalt	1.8	3×10^2	film	26
Mg ₂ NbN ₃	rocksalt	2.1	1×10^2	film	26
				bulk	159
Mg ₂ TaN ₃	rocksalt			film	26
MgMoN ₂	rocksalt			film	
	rocksaline			film	
	rocksaline			bulk	159
MgWN ₂	rocksalt			film	
	rocksaline			film	
MgGeN ₂	wurtzite		$>10^5$	film	
MgSnN ₂	wurtzite	2.0		film	88
Mg ₂ SbN ₃	wurtzite		$>10^5$	film	111
ZnTiN ₂	wurtzite	1.8	10^1	film	
ZnZrN ₂	rocksalt			film	89
	h-BN			film	89
Zn ₂ NbN ₃	wurtzite	2.1	$>10^5$	film	56
Zn ₂ TaN ₃	wurtzite			film	
Zn ₃ MoN ₄	wurtzite	2.4	3×10^4	film	55
ZnGeN ₂	wurtzite	2.5	$>10^5$	film	84
ZnSnN ₂	wurtzite	1.4	10^{-1} – 10^1	film	161
Zn ₂ SbN ₃	wurtzite	1.6	6×10^0	film	149

^aThe absorption onsets are often defined as the energy at which absorption coefficient is 10^3 cm⁻¹ or 10^4 cm⁻¹, as reported in the references. The resistivity is as determined from lateral four-point probe or van der Pauw sheet resistance measurements.

X-ray diffraction and electrical properties evaluated by temperature-dependent resistivity are shown in Figure 8. These Mg-containing ternary nitrides with Ti, Zr, Hf, and Nb form in the RS-derived structure, and Zn-containing ternary nitrides with Mo, W, and Sb form in the WZ-derived structure; all exhibit antisite disorder on the cation sublattice (Figure 8a).²⁵ All the materials shown in Figure 8a have semiconducting properties, as illustrated for RS-derived Mg–TM–N in Figure 8b. However, follow-up papers showed that this simple structure and property separation shown in Figure 8 is not always the case, with Mg₂SbN₃¹¹¹ and MgSnN₂⁸⁸ crystallizing in WZ-derived structure, ZnMoN₂ being metallic⁵⁵ and ZnGeN₂ being insulating.⁸⁴ An earlier study focused on Zn–Mo–N materials showed that while sputtered semiconducting Zn₃MoN₄ and metallic ZnMoN₂ crystallize in 4-fold coordinated WZ-derived crystal structure, it is 150–200 meV/atom higher in energy compared to a layered mixed 4/6-fold coordinated WL-type ground state structure predicted for metallic ZnMoN₂.⁵⁵ In addition, a layered BN-like ZnZrN₂ structure⁸⁹ and layered metallic RL-type MgMoN₂ structure¹⁵⁹ have been synthesized. Thus, the simple WZ/RS-derived grouping of respective Zn/Mg-containing ternary nitrides (Figure 8a) and their semiconducting behavior (Figure 8b) may not be as simple as it initially appears. For deeper insight, this progress in synthesis of Zn- and Mg-containing ternary nitrides is discussed below.

4.1. Synthesis of Zn–M–N and Other Wurtzites. One effort to discover new Zn-containing nitride semiconductors combined computational screening to identify several new Zn–M–N materials, with follow-on by high-pressure synthesis of one of the predicted phases, CaZn₂N₂.²⁷ This material exhibited a mixed octahedrally/tetrahedrally coordinated layered crystal structure, a direct 1.9–2.0 eV band gap, and measured near-band gap photoluminescence. Subsequently, the same researchers have demonstrated heteroepitaxial growth of CaZn₂N₂ by MBE with 10^{13} cm⁻³ bipolar doping and 0.3 – 4.3 cm²/(V s) mobility,¹⁶² synthesized bulk polycrystalline SrZn₂N₂¹⁶³ and Ca(Mg_{1-x}Zn_x)₂N₂ solid solutions with 1.9–3.3 eV tunable band gaps and extrinsic p-type doping by Na,¹⁶⁴ and reported on sputtered YZn₃N₃ thin films.¹⁶⁵ Another group focused on high-temperature high-pressure ammonothermal synthesis¹⁶⁶ of nitridophosphates in autoclaves filled with supercritical NH₃,¹⁶⁷ including polycrystalline Zn₂PN₃ with 3.7 eV band gap and single crystal Mg₂PN₃ with 5 eV band gap, both with wurtzite-derived crystal structure where P shares the cation site with Zn or Mg.¹⁶⁸ It would be interesting to synthesize these materials in the epitaxial thin film form on lattice-matched substrates because the Mg₂PN₃ lattice constants are close to GaN (~1.5% mismatch) and the Zn₂PN₃ lattice constants are close to AlN (~0.6% mismatch)

Two previously unreported ternary compounds in the Zn–Mo–N materials system, Zn₃MoN₄ and ZnMoN₂,⁵⁵ were predicted and synthesized in the Zn–Mo–N materials system predicted in ref 25. Both Zn₃MoN₄ and ZnMoN₂ compositions crystallize in wurtzite-derived structures (Figure 8a), with their solid solutions having a tunable +VI/+IV valence state (Figure 9a), a term coined “redox-mediated stabilization”.⁵⁵ A corresponding change in optoelectronic properties was observed in these alloys, from resistive and semitransparent Zn₃MoN₄ with a semiconducting band structure, to conductive and absorptive ZnMoN₂ with a metallic band structure. Similar to Zn₃MoN₄, Zn₃WN₄ and Zn₃(Mo_{1-x}W_x)N₄ solid solutions have been synthesized and characterized.¹⁶⁹ Subsequently, a large change in resistivity and a concomitant +IV/+III change in the

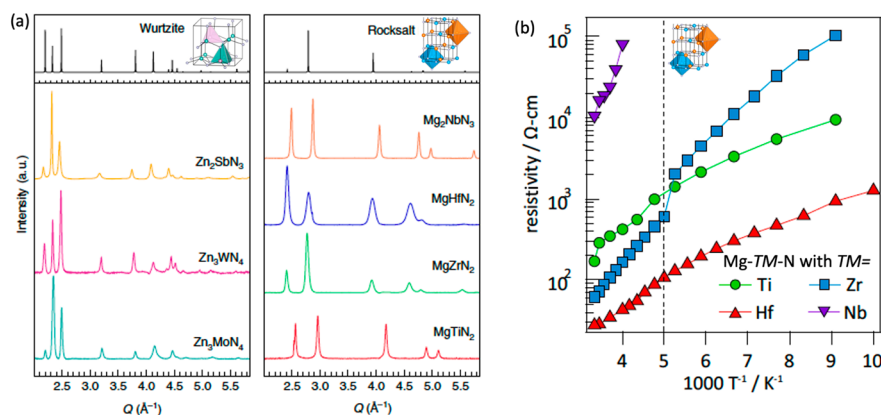


Figure 8. Experimentally synthesized ternary metal nitrides: (a) measured XRD patterns of Zn–M–N with wurtzite-type structure and Mg–M–N with rocksalt-type structure, all synthesized by cosputtering in thin film form. Adapted with permission from ref 25. Copyright 2019 Spring Nature. (b) Temperature-dependent resistivity measurement of Mg–TM–N with RS-derived structure, supporting semiconducting character of these materials. Adapted with permission from ref 26. Copyright 2019 National Academy of Sciences.

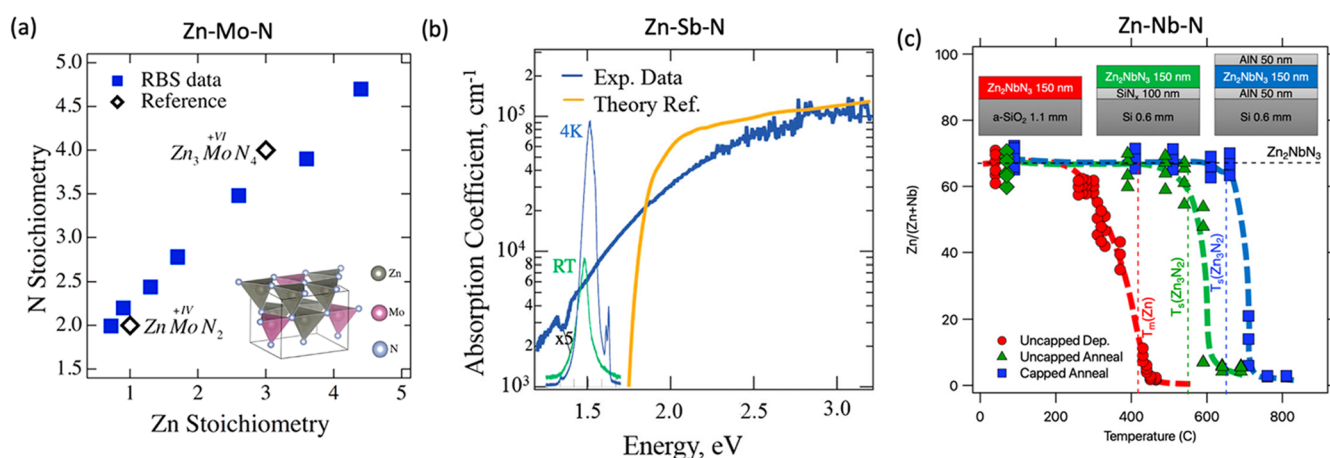


Figure 9. Experimental synthesis of Zn–M–N and other wurtzite nitrides. (a) Measured Zn–Mo–N composition of Zn and N normalized to Mo = 1, showing smooth change between stable Mo(+VI) and metastable Mo(+IV) valence states in the wurtzite structure (inset). Adapted with permission from ref 55. Copyright 2018 American Chemical Society. (b) Measured absorption spectrum of metastable wurtzite Zn₂SbN₃ compared to theoretical prediction, showing optical band gap in the 1.4–1.5 eV range, and near-band-edge photoluminescence. Adapted with permission from ref 149. Copyright 2019 Royal Society of Chemistry. (c) Measured cation composition of Zn–Nb–N samples as a function of annealing or deposition temperature, with the stoichiometric Zn₂NbN₃ composition, sublimation temperature of Zn₂N₂, and melting temperature of Zn marked by dashed lines for the three different Zn–Nb–N sample stacks. Reprinted with permission from ref 56. Copyright 2021 IOP Publishing.

valence state of Zr were observed in Mg_xZr_{2–x}N₂ solid solutions between MgZrN₂ and ZrN, both with RS-derived crystal structure.^{160,170} The differences in crystal structure (WZ vs RS), chemical system (Zn–Mo–N vs Mg–Zr–N), and stoichiometry (1–1–2 to 3–1–4 vs 0–1–1 to 1–1–2) support the generality of redox-mediated stabilization among transition metal-containing ternary nitrides.

Thin film synthesis efforts also resulted in Zn₂SbN₃ material in the Zn–Sb–N material system,¹⁴⁹ which was computationally predicted in ref 25. This Zn₂SbN₃ with WZ-derived crystal structure (Figure 8a) is the first reported crystalline Sb-containing nitride where Sb is a cation, as opposed to previously known antimonide–nitride Mg₃SbN where Sb is an anion.¹⁷¹ This Zn₂SbN₃ features an unusually high Sb (+V) valence state and unusually low 4-fold coordination of Sb, which are difficult to achieve even in oxides.^{172,173} The WZ-like Zn–Sb–N thin films with varying cation stoichiometry can be synthesized by reactive cosputtering under a wide range of processing pressures at low temperature, despite Zn₂SbN₃ being metastable with respect to nitrogen evolution according to theoretical

calculations.¹⁴⁹ This newly synthesized Zn₂SbN₃ material has a measured 1.4–1.5 eV optical absorption onset and shows room-temperature near-band-edge photoluminescence (Figure 9b). A similar reactive cosputtering synthesis approach has been successful for a metastable Mg₂SbN₃ compound in a much broader range of compositions compared to the stable antiperovskite phase Mg₃SbN.¹¹¹ This Mg₂SbN₃ has a predicted 3.1 eV direct band gap, suggesting the possibility of wurtzite (Zn_{1–x}Mg_x)₂SbN₃ solid solutions with tunable optoelectronic properties and small change in the lattice constant close to GaN (001) and ZrN (111). This work expanded the range of the Zn- and Mg-based multivalent ternary nitride based main group elements from group IV semimetals like Sn (ZnSnN₂,¹⁵⁷ MgSnN₂⁸⁸) and Ge (ZnGeN₂,⁸⁴ MgGeN₂) to group V semimetals like Sb (Zn₂SbN₃,¹⁴⁹ Mg₂SbN₃¹¹¹).

We recently synthesized and characterized a Zn₂NbN₃ ternary nitride semiconductor with wurtzite-derived crystal structure⁵⁶ that was computationally predicted in both ref 25 and ref 27. The Zn₂NbN₃ thin films were synthesized using a one-step adsorption-controlled growth that leads to *c*-axis oriented films

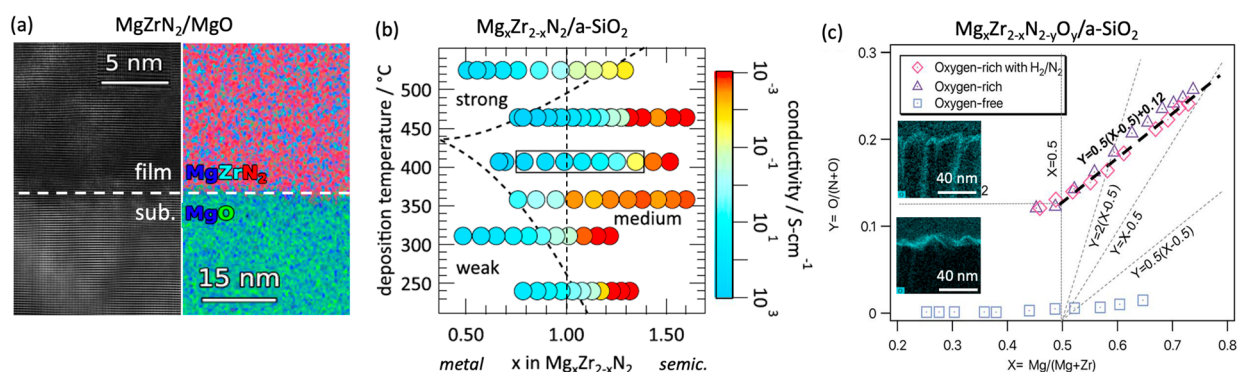


Figure 10. Experimental synthesis of rocksalt Mg–TM–N nitrides. (a) Microscopy images for MgZrN₂ films grown on (111) MgO substrates, showing a structurally and chemically sharp interface. Reprinted with permission from ref 184. Copyright 2020 AIP Publishing. (b) Electrical conductivity of Mg_xZr_{2-x}N₂ as a function of x and deposition temperature, showing a large decrease at Mg-rich compositions. Adapted with permission from ref 160. Copyright 2019 The Japan Society of Applied Physics. (c) Chemical composition and microstructure (inset) of Mg_xZr_{2-x}N₂ with and without oxygen substitution, showing correlation in cation and anion content and oxygen segregation at the surfaces and in grain boundaries. Adapted with permission from ref 170. Copyright 2020 Royal Society of Chemistry.

and a two-step deposition/annealing method with a protective layer¹⁷⁴ that suppresses the loss of Zn and N and results in polycrystalline samples suitable for crystal structure determination (Figure 9c). Measurements indicate that this sputtered Zn₂NbN₃ crystallizes in a cation-disordered wurtzite-derived structure, similar to Zn₂SbN₃ and Zn₃MoN₄. The same two-step synthesis method was used, and a similar wurtzite-derived structure was observed for Zn₂TaN₃ (unpublished results). A related sputtered Zn₂VN₃ material has been also reported by another group.¹⁷⁵ The experimentally estimated wurtzite lattice parameter ratio of Zn₂NbN₃ is $c/a = 1.55$, and the measured optical absorption onset is at $E_g^{\text{opt}} = 2.1$ eV. Both of these values are lower compared to published Zn₂NbN₃ computational values of $c/a = 1.62$ and $E_g = 3.5$ – 3.6 eV.²⁷ Theoretical calculations indicate that this difference is due to cation disorder rather than oxygen incorporation in experimental samples. This finding suggests a cation-disorder approach to tune the structural parameters and the resulting properties in Zn₂NbN₃ and possibly other multivalent ternary nitride materials. It is also interesting to note that the calculated 3.5 eV band gap of Zn₂NbN₃ is significantly larger than the calculated 1.7 eV band gap of Zn₂SbN₃, while their hexagonal lattice constants differ by only 0.2%. This suggests that the Zn₂(Nb,Sb)N₃ semiconductor alloys and Zn₂SbN₃/Zn₂NbN₃ low-strain superlattices may be used for the design of light emitting diodes and lasers to address the miscibility gap problems of (In, Ga)N or (Al, In)N alloys and lattice mismatch issues with InN/GaN or AlN/InN heterostructures, respectively.

4.2. Synthesis of Mg–M–N Rocksalt Nitrides. Prior computational and experimental work on Mg-containing ternary nitrides primarily considered the Mg–Ti–N materials system, focusing on Mg substitution into TiN.¹⁷⁶ The (Mg_xTi_{1-x})N alloys with $x = 0.0$ – 0.5 have been epitaxially grown by reactive sputtering on MgO(001) as a function of thickness in the 30–300 nm range, showing that the material is fully strained up to 60–100 nm thickness depending on x .¹⁷⁷ Another paper from the same group reported an $\sim 100\times$ increase in electrical resistivity from ~ 10 to ~ 3200 $\mu\text{Ohm cm}$ with measured optical absorption minima in the 1.7–2.0 eV range for (Mg_xTi_{1-x})N solid solutions, suggesting an extrapolated band gap of 0.7–1.7 eV for semiconducting Ti_{0.5}Mg_{0.5}N.¹⁷⁸ These experimental reports followed a computational prediction of thermodynamic stability, crystal structure, and electronic properties of MgTMN₂

(TM = Ti, Zr, Hf) compounds.^{69,109} Phase transformations¹⁷⁹ and plasmonic properties¹⁸⁰ of the (Mg_xTi_{1-x})N alloys have also been reported. Until recently, TMs in the highest oxidation state had not been incorporated in Mg–TM–N compounds, but MgMoN₂ with a lowered Mo (+IV) oxidation state has been synthesized in bulk form.^{181,136} In addition, solid state syntheses of MgTa₂N₃ and Mg₂Ta₂N₄ have been reported¹⁸² and studied for Mg deintercalation,⁵⁸ which has a reduced Ta valence state compared to Ta (+V) in a charge-balanced Mg₂Ta₂N₃ composition.

Our initial Mg–TM–N synthesis work focused on stoichiometric, charge-balanced rocksalt compounds MgTMN₂ (TM = Ti, Zr, Hf, Nb), which were prepared as thin films by sputtering from Mg and TM targets in a reactive nitrogen atmosphere.²⁶ The resulting samples show X-ray diffraction peaks consistent with a simple rocksalt structure indicating mixed occupancy of cation sites (Figure 8a). These thin film results are consistent with the bulk synthesis of MgZrN₂¹⁸³ and Mg₂NbN₃¹⁵⁹ compounds that were very recently reported. Optoelectronic characterization results show that Mg-rich compositions of the thin films are nondegenerate semiconductors with visible-range optical absorption onsets (1.8 to 2.1 eV) and up to 100 cm²/(V s) electron mobility, even for cation-disordered MgZrN₂ thin films grown by sputtering on MgO substrates with $>8\%$ lattice mismatch. Subsequent epitaxial growth of MgZrN₂ thin films on (100) and (111) MgO substrates and (001) GaN templates resulted in sharp MgZrN₂/MgO interfaces (Figure 10a). XRD rocking curves showed a full-width at half-maximum down to 0.3–0.5° for (001) GaN and (100) MgO,¹⁸⁴ which is very low for sputtered thin films. These epitaxial layers showed room-temperature Seebeck coefficients of -80 $\mu\text{V/K}$ and electron concentration of 10^{19} – 10^{20} cm⁻³ depending on orientation, albeit with lower 1–4 cm²/(V s) mobility than in earlier experiments due to carbon contamination.

Our subsequent synthesis work considered the effects of cation off-stoichiometry and oxygen content in MgZrN₂. Polycrystalline sputtered Mg_xZr_{2-x}N₂ thin films were studied, maintaining rocksalt-derived crystal structure across a broad range of Mg/Zr compositions ($0.5 \leq x \leq 1.8$) with low oxygen contents ($<1\%$ up to $x = 1$).¹⁶⁰ These samples showed tunable electrical resistivity by at least a factor of 10^6 as a function of x in Mg_xZr_{2-x}N₂ (Figure 10b). An alloy stability model was introduced, wherein Zr redox stabilizes the alloy along the

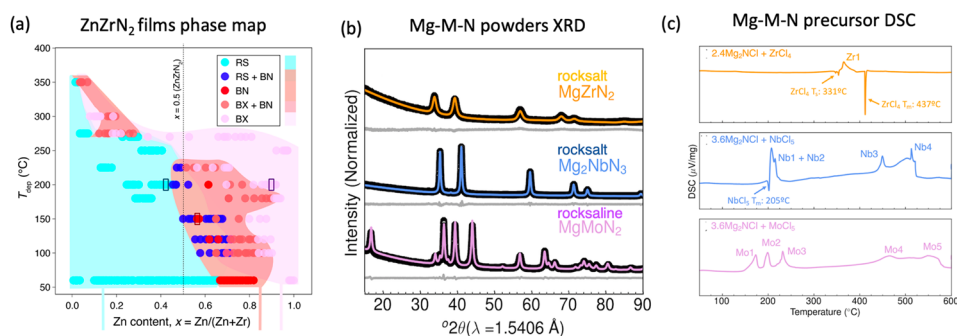


Figure 11. Experimental synthesis of layered ternary nitrides: (a) Experimental synthesis diagram for Zn–Zr–N thin films showing the phase stability regions or rocksalt-like and boron nitride-like structure. Adapted with permission from ref 89, under CC BY 4.0 license. (b) XRD patterns for three Mg–M–N powders, including MgMoN₂ with rocksaline structure as well as MgZrN₂ and Mg₂NbN₃ with rocksalt-like structure, and (c) DSC measurements for MgZrN₂, Mg₂NbN₃, and MgMoN₂, with endotherms correlating to melting transitions of metal halide precursors and exotherms corresponding to bond formation of ternary nitride products. Adapted with permission from ref 159. Copyright 2021 American Chemical Society.

ZrN–MgZrN₂ tie line and oxygen along the MgZrN₂–MgO tie line. Subsequently, the influence of oxygen and hydrogen on structure and properties of Mg_xZr_{2–x}N₂ alloys were investigated.¹⁷⁰ The excess oxygen during deposition correlates with Mg content x (Figure 10c) in agreement with the alloy model and surprisingly improves crystallinity. Hydrogen led to formation of MgO-rich grain boundaries (Figure 10c, inset) in polycrystalline Mg_xZr_{2–x}N₂ thin films with reduced electron density down to 10¹⁴ cm^{–3}. Follow up work is in progress on the synthesis of group V and group VI *TM*-containing Mg–*TM*–N materials such as Mg₃MoN₄ and Mg₂TaN₃ with predicted wurtzite-derived structures, as well as composition-dependent properties of Mg–*TM*–N materials.

4.3. Synthesis of Layered Nitrides. In addition to Zn–M–N and Mg–M–N with 3D wurtzite-like or rocksalt-like crystal structures, several 2D layered nitrides have been reported in bulk powder form. For example, MgTa₂N₃¹⁸⁵ and MgMoN₂¹⁸¹ have been synthesized using Mg(NH)₂ or Mg+NaN₃ at high pressure and from Mg₃N₂ precursors at high temperature and studied for divalent battery applications.^{58,136} Both of these layered ternary nitride materials have reduced valence states of the transition metal, such as Ta(III/IV) and Mo(IV), which leads to metallic character of these compounds and may result in interesting topological properties. For example, MgTa₂N₃ has been predicted to be a Dirac semimetal with the Fermi level located at the Dirac point,¹⁸⁶ and it transforms into a Weyl semimetal with increasing Nb concentration in MgTa_{2–x}Nb_xN₃ alloys.¹⁸⁷ In contrast to these Mg–M–N ternary nitrides, there are no experimental reports on either bulk or thin film synthesis of Zn–M–N ternary nitrides with 2D layered crystal structures.

Our initial attempts to synthesize layered ternary nitrides in thin film form started with ZnZrN₂ in thin film form,⁸⁹ which was predicted to crystallize in wurtzite structure, comprised of 2D “wurtzite” and “rocksalt” layers (Figure 4a), by three separate theoretical studies.^{25,27,108} Hundreds of Zn_xZr_{1–x}N_y thin film samples were synthesized using combinatorial sputtering at elevated temperatures, and we also attempted annealing Zn–Zr–N precursors that were deposited at ambient temperature. According to both in-house and synchrotron XRD measurements (Figure 11a), both in-house and at synchrotron, these Zn–Zr–N thin films crystallize in either a metastable 3D rocksalt-derived structure at the Zr-rich composition or 2D boron nitride-derived structure at Zn-rich cation composition, rather than the theoretically predicted layered wurtzite structure

at the stoichiometric ZnZrN₂ composition. This is in contrast to ZnTiN₂ which was both predicted and synthesized in the wurtzite-derived crystal structure (unpublished results). These experimental and theoretical results are reconciled by statistical polymorph sampler calculations¹⁸⁸ at ZnZrN₂ stoichiometry showing that rocksalt- and boron nitride-derived structures become more stable above the ensemble temperature of ~1000 K. This theoretically predicted transition temperature is higher than the measured substrate temperature during the sputtering but lower than 2000–3000 K effective temperature^{152,116,83} that corresponds to kinetically quenched disorder during the sputter deposition process (Figure 7). Additional calculations show that these two structures become more stable than the wurtzite structure in the presence of disorder because of higher energetic tolerance to cation cross-substitution at ZnZrN₂ composition and higher energetic tolerance to off-stoichiometry.

Subsequent work on layered ternary nitrides focused on MgMoN₂ in bulk form,¹⁵⁹ which had been experimentally demonstrated in layered rocksalt (RL) structure by two distinct bulk synthesis methods, at high temperatures in a tube furnace and high pressures in autoclaves.^{136,181} Bulk powder MgMoN₂ as well as MgZrN₂ and Mg₂NbN₃ were synthesized at NREL using an ion-exchange bulk synthesis method from a Mg₂NCl mixed-anion nitrogen source and MoCl₅ transition metal precursors using gentler conditions (Figure 11b),¹⁵⁹ similar to the synthesis route known for binary Mn₃N₂ nitrides¹⁸⁹ and used for the MgZrN₂ synthesis.¹⁸³ According to DSC measurements (Figure 11c), this synthesis approach is enabled by a two-step temperature profile of the reaction, with short-range nucleation at lower temperature (300–450 °C), and subsequent long-range crystallization at higher temperature (800–900 °C). The XRD measurements of these bulk powder MgMoN₂ samples confirm the rocksaltine crystal structure featuring alternating octahedral (Oh) and trigonal prismatic (Tp) layers and indicate some degree of Mg/Mo cation disorder of Mo off-stoichiometry. We are also observing a greater Mg/M cation disorder in Oh/Tp site-ordered rocksaltine MgMoN₂ and related MgWN₂ thin films synthesized by nucleation from rocksalt precursors (unpublished results). These experimental results make MgMoN₂ and MgWN₂ some of few ternary nitrides that have been made in film and in bulk forms, and where site disorder (Oh vs Tp) and elemental disorder (Mg vs *TM*) can be controlled to some extent. Moving forward, these MgMoN₂ and MgWN₂ model systems may enable new understanding on the effects of synthesis routes on polymorph stability and thus help

to better elucidate the effects of cation disorder on material properties.

4.4. Discussion of Experimental Synthesis. It is interesting to note some separation of the ternary nitride materials synthesized in bulk and thin film forms. For example, some Mg-based Mg–M–N have been synthesized only in the thin film form,^{26,111} whereas there are only bulk synthesis reports of some Ca-, Sr-, and Ba-containing materials.^{79,190} Within the Zn-based Zn–M–N material family, Zn₂SbN₃¹⁴⁹ has been synthesized only in thin film form, and Zn₂PN₃ is an example of material synthesized only in bulk.¹⁶⁷ Some of this material separation between film and bulk forms may be related to the synthesis considerations and preferences. On one hand, certain elements are considered prohibitive (e.g., P) or difficult (e.g., Zn) to use as precursors in nondedicated vacuum deposition equipment because of potential cross-contamination issues. On the other hand, in bulk synthesis methods some elemental precursors tend to decompose before they melt (e.g., Mg₃N₂) while other elements are very challenging to nitridize (e.g., Sb). However, there are several exceptions to this film/bulk separation trend, with CaZn₂N₂^{27,164} and MgSnN₂^{86,88} synthesized in forms of both bulk and thin film samples, similar to more-established ZnSnN₂^{85,191} and ZnGeN₂^{78,84} materials. We have also reported bulk synthesis of MgZrN₂, Mg₂NbN₃, and MgMoN₂,¹⁵⁹ following our earlier thin film synthesis report.²⁶ Having both bulk (powder or crystal) and thin film (polycrystalline or epitaxial) samples is advantageous because they lend themselves to different characterization methods. On one hand, structural refinement with X-rays or neutron diffraction and related cation ordering studies are easier with bulk materials, and having large enough single crystals enables very accurate band gap and carrier mobility measurements, if suitable Ohmic contacts can be achieved. On the other hand, thin films provide a better and easier measure of electronic properties compared to bulk powders, though often not as good as perfect single crystals, can be more easily integrated with other materials, and thus are often considered more “technologically relevant”. Our hope is that this review will help bridge the gap between groups doing synthesis and characterization in bulk and thin film forms and lead to more materials cases where information from these complementary experiments can be compared with each other.

Another notable point is the difficulty of experimental synthesis of ternary nitrides with layered WS, RL, WL, and BN structures. Our initial thin film synthesis attempts have resulted in Mg₂NbN₃ with 3D RS instead of 2D BN structure and ZnZrN₂ with 3D RS or WZ instead of 2D WS crystal structures, regardless of chemical composition or growth conditions. However, since WZ, BN, and WS have hexagonal symmetry, their structures may be difficult to distinguish by XRD, especially for preferentially oriented thin films. In the literature, other ternary nitrides that are structurally and chemically related to WS-ZnZrN₂ have been reported in bulk form. For example, FeWN₂ and MnMoN₂ synthesized by ammonolysis of oxide precursors at 800–900 °C¹⁹² crystallize in what can be viewed as a “wurtzeline” (WL) crystal structure composed of Fe/Mn in tetrahedral coordination similar to wurtzite (WZ) structure type and Mo/W in trigonal prismatic coordination similar to nickeline (NC) structure type. As another example, hexagonal boron nitride (h-BN) with the binary prototype structure of the ternary BN-derived Mg₂NbN₃ is also typically synthesized from oxide or hydroxide precursors by ammonolysis reaction above 900 °C.¹⁹³ These literature

reports suggest that higher synthesis temperatures may be necessary to stabilize the predicted BN-type Mg₂NbN₃ and WS-type ZnZrN₂ materials and control cation ordering in such materials. Indeed, it seems possible to synthesize thin films of MgMoN₂ and MgWN₂ with layered crystal structures of alternating octahedral and trigonal prismatic sites occupied by Mg and TM with different degrees of ordering (unpublished results). More experimental work using kinetically controlled growth¹⁹⁴ with in situ characterization methods,¹⁹⁵ such as cation-exchange metathesis reactions,^{159,183} nucleation from atomically dispersed precursors,^{174,56} and modulated exposure of metal plumes in a growth chamber,^{196,197} is in progress to understand and control both site ordering and cation ordering in layered multivalent ternary nitride materials.

5. SUMMARY AND CONCLUSIONS

This article describes the authors' perspective on multivalent ternary nitride materials defined herein, with particular focus on progress with experimental synthesis of theoretically predicted Zn- and Mg-containing compounds. The intermediate ionic/covalent bonding properties of nitrogen lead to several favorable functional properties of nitride materials, with some of the known inorganic nitrides having technological applications. Prototypical examples among binary nitrides are main group nitrides with wurtzite crystal structures (e.g., AlN, GaN, and InN semiconductors) and transition metal nitrides with rocksalt crystal structures, including both semiconductors (e.g., ScN, YN, LaN) and metals (e.g., TiN, ZrN, NbN), all often grown as thin films for practical applications. A slew of ternary nitride semiconductors with a nominal A²⁺B⁴⁺N₂³⁻ charge balance and A = Ba, Sr, Ca, and B = Si, Ge, Ti, Zr, Hf are also known to inorganic chemists and occasionally studied for energy applications in bulk powder form. With advances in the synthesis science of nitride thin films, these materials' discovery and property utilization trends in ternary nitride materials are likely to expand.

There has been a significant progress in computational predictions and experimental synthesis of the Zn- and Mg-based ternary nitride materials over the past 5 years. Theoretical studies, including both broad surveys and detailed calculations, predicted hundreds of new ternary nitride materials. Experimental studies closely followed the theory, with tens of the newly predicted Zn- and Mg-based ternary nitrides synthesized and characterized—a huge acceleration compared to historical rate of approximately two to three materials per year. The synthesized multivalent ternary nitrides include not only materials with equal cations quantities of A²⁺:B⁴⁺ = 1:1 as in ABN₂ but also those with A²⁺:B⁵⁺ = 2:1 as in A₂BN₃ and A²⁺:B⁶⁺ = 3:1 as in A₃BN₄, allowing for a broader range of elements to be incorporated (e.g., B = Nb, Ta, Mo, W, Sb, etc.). Other examples of experimental advances for ternary nitrides include expansion of wurtzite-derived materials from main group to transition metal elements and extension of rocksalt-derived materials from metals to semiconductors. This computational and experimental progress has led to better understanding of composition–structure–property relationships in nitride materials and resulted in realization of several metastable ternary nitrides.

Moving forward, we expect that some of these new multivalent ternary nitride materials synthesized in the past decade will see an increase in research activity due to interest in their practical applications. One important scientific challenge will be to better understand the origins and effects of cation disorder in these compounds and to develop increased control

of ordering to influence the resulting properties. Another fruitful future basic research direction would be in thin film synthesis of multivalent ternary nitride with layered crystal structures, outside of the more common 3D bonded wurtzite-derived and rocksalt-derived materials. Here, better understanding of the enthalpic and entropic contributions to polymorph stabilization, as well as kinetically controlled synthesis methods that can overcome these thermodynamic limitations, would be of great value. Finally, we hope to translate the materials chemistry lessons learned from the theoretical prediction and experimental synthesis of multivalent ternary nitrides to other classes of inorganic solid state compounds.

■ ASSOCIATED CONTENT

SI Supporting Information

The Supporting Information is available free of charge at <https://pubs.acs.org/doi/10.1021/acs.chemmater.1c03014>.

Alternative structure maps for ternary metal nitrides (Figure S1) and predicted electronic structure properties of nitrides (Figure S2) (PDF)

■ AUTHOR INFORMATION

Corresponding Author

Andriy Zakutayev – *Materials Science Center, National Renewable Energy Laboratory, Golden, Colorado 80401, United States*; orcid.org/0000-0002-3054-5525;
Email: andriy.zakutayev@nrel.gov

Authors

Sage R. Bauers – *Materials Science Center, National Renewable Energy Laboratory, Golden, Colorado 80401, United States*;
orcid.org/0000-0002-6505-5016

Stephan Lany – *Materials Science Center, National Renewable Energy Laboratory, Golden, Colorado 80401, United States*;
orcid.org/0000-0002-8127-8885

Complete contact information is available at:
<https://pubs.acs.org/doi/10.1021/acs.chemmater.1c03014>

Notes

The views expressed in this article do not necessarily represent the views of the DOE or the U.S. Government.

The authors declare no competing financial interest.

Biographies

Andriy Zakutayev is a scientist at the National Renewable Energy Laboratory (NREL), leading efforts to discover and design new inorganic solid state materials for advanced energy technologies. He is a recipient of the DOE Early Career Award on “Kinetic Synthesis of Metastable Nitrides” from the U.S. Department of Energy. Dr. Zakutayev has worked at NREL since 2010 when he joined as a postdoc with Dr. David Ginley, after he received his Ph.D. in Physics in 2010 from Oregon State University working with Prof. Janet Tate on wide-band gap p-type semiconductors for optoelectronic applications. Prior to his graduate studies, Andriy received a B.S. in Electronics in 2006 from Lviv Polytechnic National University (Ukraine).

Sage Bauers is a scientist at NREL, where he works on materials design, discovery, and device integration. Prior to his current role, he was a postdoc at NREL, working with Andriy Zakutayev on discovery of new ternary nitride semiconductors. Dr. Bauers received his Ph.D. in Chemistry from the University of Oregon in 2016, where he designed chalcogenide superlattices for thermoelectric applications with guidance from Prof. David Johnson. He has also held multiple positions

in the semiconductor manufacturing industry, focusing on both device design and fabrication process R&D.

Stephan Lany joined NREL in 2003 as a postdoctoral researcher with Dr. Alex Zunger and has been a staff scientist since 2006. He works on first-principles modeling of real, nonideal materials with a current focus on structure prediction for crystals and interfaces, thermochemistry and defect equilibria, and electronic structure properties of disordered systems. Dr. Lany received his Ph.D. in Physics in 2002 from the Universitat des Saarlandes, where he investigated II–VI semiconductors with DFT calculations to complement the experimental studies in the group of Prof. Th. Wichert.

■ ACKNOWLEDGMENTS

This work was funded by the U.S. Department of Energy (DOE), Office of Science (SC), Office of Basic Energy Sciences (BES), Materials Chemistry program, as a part of the Early Career Award “Kinetic Synthesis of Metastable Nitrides”. It used high-performance computing resources located at the National Renewable Energy Laboratory (NREL) and sponsored by the Office of Energy Efficiency and Renewable Energy. The authors would like to thank Brooks M. Tellekamp, Paul K. Todd, and Rachel Woods-Robinson for useful comments to an early draft of this manuscript. The Alliance for Sustainable Energy, LLC, operates NREL for the DOE under Contract No. DE-AC36-08GO28308.

■ REFERENCES

- (1) Belsky, A.; Hellenbrandt, M.; Karen, V. L.; Luksch, P. New Developments in the Inorganic Crystal Structure Database (ICSD): Accessibility in Support of Materials Research and Design. *Acta Crystallogr. B Struct. Sci.* **2002**, *58* (3), 364–369.
- (2) Kohn, W.; Sham, L. J. Self-Consistent Equations Including Exchange and Correlation Effects. *Phys. Rev.* **1965**, *140* (4A), A1133.
- (3) Perdew, J. P.; Burke, K.; Ernzerhof, M. Generalized Gradient Approximation Made Simple [Phys. Rev. Lett. **77**, 3865 (1996)]. *Phys. Rev. Lett.* **1997**, *78* (7), 1396–1396.
- (4) Jain, A.; Ong, S. P.; Hautier, G.; Chen, W.; Richards, W. D.; Dacek, S.; Cholia, S.; Gunter, D.; Skinner, D.; Ceder, G.; Persson, K. A. Commentary: The Materials Project: A Materials Genome Approach to Accelerating Materials Innovation. *APL Mater.* **2013**, *1* (1), 011002.
- (5) Curtarolo, S.; Setyawan, W.; Wang, S.; Xue, J.; Yang, K.; Taylor, R. H.; Nelson, L. J.; Hart, G. L. W.; Sanvito, S.; Buongiorno-Nardelli, M.; Mingo, N.; Levy, O. AFLOWLIB.ORG: A Distributed Materials Properties Repository from High-Throughput Ab Initio Calculations. *Comput. Mater. Sci.* **2012**, *58*, 227–235.
- (6) Kirklin, S.; Saal, J. E.; Meredig, B.; Thompson, A.; Doak, J. W.; Aykol, M.; Rühl, S.; Wolverton, C. The Open Quantum Materials Database (OQMD): Assessing the Accuracy of DFT Formation Energies. *npj Comput. Mater.* **2015**, *1* (1), 1–15.
- (7) Curtarolo, S.; Hart, G. L. W.; Nardelli, M. B.; Mingo, N.; Sanvito, S.; Levy, O. The High-Throughput Highway to Computational Materials Design. *Nat. Mater.* **2013**, *12* (3), 191–201.
- (8) Hautier, G.; Jain, A.; Ong, S. P. From the Computer to the Laboratory: Materials Discovery and Design Using First-Principles Calculations. *J. Mater. Sci.* **2012**, *47* (21), 7317–7340.
- (9) Zunger, A. Inverse Design in Search of Materials with Target Functionalities. *Nat. Rev. Chem.* **2018**, *2* (4), 1–16.
- (10) Alberi, K.; Nardelli, M. B.; Zakutayev, A.; Mitas, L.; Curtarolo, S.; Jain, A.; Fornari, M.; Marzari, N.; Takeuchi, L.; Green, M. L.; Kanatzidis, M.; Toney, M. F.; Butenko, S.; Meredig, B.; Lany, S.; Kattner, U.; Davydov, A.; Toberer, E. S.; Stevanovic, V.; Walsh, A.; Park, N.-G.; Aspuru-Guzik, A.; Tabor, D. P.; Nelson, J.; Murphy, J.; Setlur, A.; Gregoire, J.; Li, H.; Xiao, R.; Ludwig, A.; Martin, L. W.; Rappe, A. M.; Wei, S.-H.; Perkins, J. The 2019 Materials by Design Roadmap. *J. Phys. D: Appl. Phys.* **2019**, *52* (1), 013001.

- (11) Kovnir, K. Predictive Synthesis. *Chem. Mater.* **2021**, *33* (13), 4835–4841.
- (12) Kalil, T.; Wadia, C. *Materials Genome Initiative for Global Competitiveness*; 2011.
- (13) Green, M. L.; Choi, C. L.; Hatrick-Simpers, J. R.; Joshi, A. M.; Takeuchi, I.; Barron, S. C.; Campo, E.; Chiang, T.; Empedocles, S.; Gregoire, J. M.; Kusne, A. G.; Martin, J.; Mehta, A.; Persson, K.; Trautt, Z.; Van Duren, J.; Zakutayev, A. Fulfilling the Promise of the Materials Genome Initiative with High-Throughput Experimental Methodologies. *Appl. Phys. Rev.* **2017**, *4* (1), 011105.
- (14) DiSalvo, F. J. Solid-State Chemistry: A Rediscovered Chemical Frontier. *Science* (80-) **1990**, *247* (4943), 649–655.
- (15) Juza, R.; Langer, K.; Von Benda, K. Ternary Nitrides, Phosphides, and Arsenides of Lithium. *Angew. Chemie Int. Ed.* **1968**, *7* (5), 360–370.
- (16) DiSalvo, F. J.; Clarke, S. J. Ternary Nitrides: A Rapidly Growing Class of New Materials. *Curr. Opin. Solid State Mater. Sci.* **1996**, *1* (2), 241–249.
- (17) Niewa, R.; DiSalvo, F. J. Recent Developments in Nitride Chemistry. *Chem. Mater.* **1998**, *10* (10), 2733–2752.
- (18) Marchand, R. Ternary and Higher Order Nitride Materials. In *Handbook on the Physics and Chemistry of Rare Earths*; Elsevier: 1998; Vol. 25, pp 51–99, .
- (19) Zakutayev, A. Design of Nitride Semiconductors for Solar Energy Conversion. *J. Mater. Chem. A* **2016**, *4* (18), 6742–6754.
- (20) Greenaway, A. L.; Melamed, C. L.; Tellekamp, M. B.; Woods-Robinson, R.; Toberer, E. S.; Neilson, J. R.; Tamboli, A. C. Ternary Nitride Materials: Fundamentals and Emerging Device Applications. *Annu. Rev. Mater. Res.* **2021**, *51*, 591–618.
- (21) Niewa, R. *Ammonothermal Synthesis and Crystal Growth of Nitrides*; Meissner, E., Niewa, R., Eds.; Springer Series in Materials Science; Springer International Publishing: 2021; Vol. 304.
- (22) Horvath-Bordon, E.; Riedel, R.; Zerr, A.; McMillan, P. F.; Auffermann, G.; Prots, Y.; Bronger, W.; Knier, R.; Kroll, P. High-Pressure Chemistry of Nitride-Based Materials. *Chem. Soc. Rev.* **2006**, *35* (10), 987.
- (23) Zakutayev, A.; Zhang, X.; Nagaraja, A.; Yu, L.; Lany, S.; Mason, T. O.; Ginley, D. S.; Zunger, A. Theoretical Prediction and Experimental Realization of New Stable Inorganic Materials Using the Inverse Design Approach. *J. Am. Chem. Soc.* **2013**, *135* (27), 10048–10054.
- (24) Dahlqvist, M.; Tao, Q.; Zhou, J.; Palisaitis, J.; Persson, P. O. Å.; Rosen, J. Theoretical Prediction and Synthesis of a Family of Atomic Laminate Metal Borides with In-Plane Chemical Ordering. *J. Am. Chem. Soc.* **2020**, *142* (43), 18583–18591.
- (25) Sun, W.; Bartel, C. J.; Arca, E.; Bauers, S. R.; Matthews, B.; Orvañanos, B.; Chen, B. R.; Toney, M. F.; Schelhas, L. T.; Tumas, W.; Tate, J.; Zakutayev, A.; Lany, S.; Holder, A. M.; Ceder, G. A Map of the Inorganic Ternary Metal Nitrides. *Nat. Mater.* **2019**, *18* (7), 732–739.
- (26) Bauers, S. R.; Holder, A.; Sun, W.; Melamed, C. L.; Woods-Robinson, R.; Mangum, J.; Perkins, J.; Tumas, W.; Gorman, B.; Tamboli, A.; Ceder, G.; Lany, S.; Zakutayev, A. Ternary Nitride Semiconductors in the Rocksalt Crystal Structure. *Proc. Natl. Acad. Sci. U. S. A.* **2019**, *116* (30), 14829–14834.
- (27) Hinuma, Y.; Hatakeyama, T.; Kumagai, Y.; Burton, L. A.; Sato, H.; Muraba, Y.; Imura, S.; Hiramatsu, H.; Tanaka, I.; Hosono, H.; Oba, F. Discovery of Earth-Abundant Nitride Semiconductors by Computational Screening and High-Pressure Synthesis. *Nat. Commun.* **2016**, *7* (1), 1–10.
- (28) Kloß, S. D.; Schnick, W. Nitridophosphates: A Success Story of Nitride Synthesis. *Angew. Chemie - Int. Ed.* **2019**, *58* (24), 7933–7944.
- (29) Lany, S. Band-Structure Calculations for the 3d Transition Metal Oxides in GW. *Phys. Rev. B - Condens. Matter Mater. Phys.* **2013**, *87* (8), 085112.
- (30) Shur, M.; Gelmont, B.; Asif Khan, M. Electron Mobility in Two-Dimensional Electron Gas in AlGaIn/GaN Heterostructures and in Bulk GaN. *J. Electron. Mater.* **1996**, *25* (5), 777–785.
- (31) Lany, S.; Zunger, A. Dual Nature of Acceptors in GaN and ZnO: The Curious Case of the Shallow MgGa Deep State. *Appl. Phys. Lett.* **2010**, *96* (14), 142114.
- (32) Varley, J. B.; Janotti, A.; Franchini, C.; Van De Walle, C. G. Role of Self-Trapping in Luminescence and p-Type Conductivity of Wide-Band-Gap Oxides. *Phys. Rev. B - Condens. Matter Mater. Phys.* **2012**, *85* (8), 081109.
- (33) Zakutayev, A.; Caskey, C. M.; Fioretti, A. N.; Ginley, D. S.; Vidal, J.; Stevanovic, V.; Tea, E.; Lany, S. Defect Tolerant Semiconductors for Solar Energy Conversion. *J. Phys. Chem. Lett.* **2014**, *5* (7), 1117–1125.
- (34) Talley, K. R.; Sherbondy, R.; Zakutayev, A.; Brennecke, G. L. Review of High-Throughput Approaches to Search for Piezoelectric Nitrides. *J. Vac. Sci. Technol. A* **2019**, *37* (6), 060803.
- (35) Morkoc, H. *Handbook of Nitride Semiconductors and Devices*; Wiley-VCH Verlag GmbH & Co. KGaA: 2009; Vol. 1, .
- (36) Pierson, H. O.; Hugh, O.; Pierson, H. O. *Handbook of Refractory Carbides and Nitrides*; William Andrew Inc.: 1996.
- (37) Fitzmaurice, J. C.; Hector, A.; Rowley, A. T.; Parkin, I. P. Rapid, Low Energy Synthesis of Lanthanide Nitrides. *Polyhedron* **1994**, *13* (2), 235–240.
- (38) Schumacher, D. P.; Wallace, W. E. Magnetic Characteristics of Some Lanthanide Nitrides. *Inorg. Chem.* **1966**, *5* (9), 1563–1567.
- (39) Widenmeyer, M.; Hansen, T. C.; Leineweber, A.; Weidenkaff, A.; Niewa, R. Nitrogen Transfer between Solid Phases in the System Mn-N Detected via in Situ Neutron Diffraction. *Zeitschrift für Anorg. und Allg. Chemie* **2017**, *643* (23), 1929–1938.
- (40) Suzuki, K.; Morita, H.; Kaneko, T.; Yoshida, H.; Fujimori, H. Crystal Structure and Magnetic Properties of the Compound FeN. *J. Alloys Compd.* **1993**, *201* (1–2), 11–16.
- (41) Lukashev, P.; Lambrecht, W. R. L. First-Principles Study of the Preference for Zinc-Blende or Rocksalt Structures in FeN and CoN. *Phys. Rev. B* **2004**, *70* (24), 245205.
- (42) Momma, K.; Izumi, F. VESTA 3 for Three-Dimensional Visualization of Crystal, Volumetric and Morphology Data. *J. Appl. Crystallogr.* **2011**, *44* (6), 1272–1276.
- (43) Zerr, A.; Miehe, G.; Riedel, R. Synthesis of Cubic Zirconium and Hafnium Nitride Having Th3P4 Structure. *Nat. Mater.* **2003**, *2* (3), 185–189.
- (44) Salamat, A.; Hector, A. L.; Gray, B. M.; Kimber, S. A. J.; Bouvier, P.; McMillan, P. F. Synthesis of Tetragonal and Orthorhombic Polymorphs of Hf3N4 by High-Pressure Annealing of a Prestructured Nanocrystalline Precursor. *J. Am. Chem. Soc.* **2013**, *135* (25), 9503–9511.
- (45) Brauer, G.; Weidlein, J. R. Synthesis and Properties of Red Tantalum Nitride Ta3N5. *Angew. Chem., Int. Ed. Engl.* **1965**, *4* (3), 241–242.
- (46) Wang, S.; Ge, H.; Sun, S.; Zhang, J.; Liu, F.; Wen, X.; Yu, X.; Wang, L.; Zhang, Y.; Xu, H.; Neuefeind, J. C.; Qin, Z.; Chen, C.; Jin, C.; Li, Y.; He, D.; Zhao, Y. A New Molybdenum Nitride Catalyst with Rhombohedral MoS2 Structure for Hydrogenation Applications. *J. Am. Chem. Soc.* **2015**, *137* (14), 4815–4822.
- (47) Higashi, T.; Nishiyama, H.; Suzuki, Y.; Sasaki, Y.; Hisatomi, T.; Katayama, M.; Minegishi, T.; Seki, K.; Yamada, T.; Domen, K. Transparent Ta3N5 Photoanodes for Efficient Oxygen Evolution toward the Development of Tandem Cells. *Angew. Chemie Int. Ed.* **2019**, *58* (8), 2300–2304.
- (48) Marchand, R.; Tessier, F.; DiSalvo, F. J. New Routes to Transition Metal Nitrides: And Characterization of New Phases. *J. Mater. Chem.* **1999**, *9* (1), 297–304.
- (49) Parkin, I. P.; Rowley, A. T. Solid-State Routes to Tantalum Nitrides (TaN, Ta3N5). *Adv. Mater.* **1994**, *6* (10), 780–782.
- (50) Yokoyama, D.; Hashiguchi, H.; Maeda, K.; Minegishi, T.; Takata, T.; Abe, R.; Kubota, J.; Domen, K. Ta3N5 Photoanodes for Water Splitting Prepared by Sputtering. *Thin Solid Films* **2011**, *519* (7), 2087–2092.
- (51) Sharan, A.; Lany, S. Computational Discovery of Stable and Metastable Ternary Oxynitrides. *J. Chem. Phys.* **2021**, *154* (23), 234706.

- (52) Martinez, A. D.; Fioretti, A. N.; Toberer, E. S.; Tamboli, A. C. Synthesis, Structure, and Optoelectronic Properties of II–IV–V2Materials. *J. Mater. Chem. A* **2017**, *5* (23), 11418–11435.
- (53) Schnepf, R. R.; Cordell, J. J.; Tellekamp, M. B.; Melamed, C. L.; Greenaway, A. L.; Mis, A.; Brenneka, G. L.; Christensen, S.; Tucker, G. J.; Toberer, E. S.; Lany, S.; Tamboli, A. C. Utilizing Site Disorder in the Development of New Energy-Relevant Semiconductors. *ACS Energy Lett.* **2020**, *5* (6), 2027–2041.
- (54) Khan, I. S.; Heinselman, K. N.; Zakutayev, A. Review of ZnSnN2 Semiconductor Material. *J. Phys. Energy* **2020**, *2* (3), 032007.
- (55) Arca, E.; Lany, S.; Perkins, J. D.; Bartel, C.; Mangum, J.; Sun, W.; Holder, A.; Ceder, G.; Gorman, B.; Teeter, G.; Tumas, W.; Zakutayev, A. Redox-Mediated Stabilization in Zinc Molybdenum Nitrides. *J. Am. Chem. Soc.* **2018**, *140* (12), 4293–4301.
- (56) Zakutayev, A. Synthesis of Zn2NbN3 Ternary Nitride Semiconductor with Wurtzite-Derived Crystal Structure. *J. Phys.: Condens. Matter* **2021**, *33* (35), 354003.
- (57) Niewa, R.; Zhrebtsov, D. A.; Schnelle, W.; Wagner, F. R. Metal-Metal Bonding in ScTaN2. A New Compound in the System ScN-TaN. *Inorg. Chem.* **2004**, *43* (20), 6188–6194.
- (58) Verrelli, R.; Black, A. P.; Frontera, C.; Oro-Sole, J.; Arroyo-De Dompablo, M. E.; Fuertes, A.; Palacín, M. R. On the Study of Ca and Mg Deintercalation from Ternary Tantalum Nitrides. *ACS Omega* **2019**, *4* (5), 8943–8952.
- (59) Lyu, S.; Lambrecht, W. R. L. Quasiparticle Self-Consistent GW Electronic Band Structure of Cd-IV-N2 Compounds. *Phys. Rev. Mater.* **2017**, *1* (2), 024606.
- (60) Shannon, R. D.; Prewitt, C. T. Revised Values of Effective Ionic Radii. *Acta Crystallogr. Sect. B Struct. Crystallogr. Cryst. Chem.* **1970**, *26* (7), 1046–1048.
- (61) Pauling, L.; Wheland, G. W. The Nature of the Chemical Bond. *V. J. Chem. Phys.* **1934**, *2* (8), 482.
- (62) Madden, P. A.; Wilson, M. ‘Covalent’ Effects in ‘Ionic’ Systems. *Chem. Soc. Rev.* **1996**, *25* (5), 339–350.
- (63) Gregory, D. H.; O’Meara, P. M.; Gordon, A. G.; Siddons, D. J.; Blake, A. J.; Barker, M. G.; Hamor, T. A.; Edwards, P. P. Layered Ternary Transition Metal Nitrides; Synthesis, Structure and Physical Properties. *J. Alloys Compd.* **2001**, *317–318*, 237–244.
- (64) Gál, Z. A.; Mallinson, P. M.; Orchard, H. J.; Clarke, S. J. Synthesis and Structure of Alkaline Earth Silicon Nitrides: BaSiN2, SrSiN2, and CaSiN2. *Inorg. Chem.* **2004**, *43* (13), 3998–4006.
- (65) Etourneau, J.; Portier, J.; Ménil, F. The Role of the Inductive Effect in Solid State Chemistry: How the Chemist Can Use It to Modify Both the Structural and the Physical Properties of the Materials. *J. Alloys Compd.* **1992**, *188* (C), 1–7.
- (66) Bruls, R. J.; Hintzen, H. T.; Metselaar, R.; Loong, C. K. Anisotropic Thermal Expansion of MgSiN2 from 10 to 300 K as Measured by Neutron Diffraction. *J. Phys. Chem. Solids* **2000**, *61* (8), 1285–1293.
- (67) Gregory, D. H.; Barker, M. G.; Edwards, P. P.; Siddons, D. J. Synthesis and Structure of Two New Layered Ternary Nitrides, SrZrN2 and SrHfN2. *Inorg. Chem.* **1996**, *35* (26), 7608–7613.
- (68) Burdett, J. K.; Lee, S.; McLarnan, T. J. Coloring Problem. *J. Am. Chem. Soc.* **1985**, *107* (11), 3083–3089.
- (69) Gharavi, M. A.; Armiento, R.; Alling, B.; Eklund, P. Theoretical Study of Phase Stability, Crystal and Electronic Structure of MeMgN2 (Me = Ti, Zr, Hf) Compounds. *J. Mater. Sci.* **2018**, *53* (6), 4294–4305.
- (70) Mather, G. C.; Dussarrat, C.; Etourneau, J.; West, A. R. A Review of Cation-Ordered Rock Salt Superstructureoxides. *J. Mater. Chem.* **2000**, *10* (10), 2219–2230.
- (71) Prots’, Y.; Niewa, R.; Schnelle, W.; Kniep, R. New Ternary Alkaline Earth Metal Cerium(IV) Nitrides: CaCeN2 and SrCeN2. *Zeitschrift für Anorg. und Allg. Chemie* **2002**, *628* (7), 1590–1596.
- (72) Niewa, R.; Vajenine, G. V.; DiSalvo, F. J.; Luob, H.; Yelon, W. B. Unusual Bonding in Ternary Nitrides: Preparation, Structure and Properties of Ce2MnN3. *Zeitschrift für Naturforsch. B* **1998**, *53* (1), 63–74.
- (73) Gregory, D. H.; Barker, M. G.; Edwards, P. P.; Siddons, D. J. Synthesis and Structure of the New Ternary Nitride SrTiN2. *Inorg. Chem.* **1998**, *37* (15), 3775–3778.
- (74) Gregory, D. H.; Barker, M. G.; Edwards, P. P.; Slaski, M.; Siddons, D. J. Synthesis, Structure, and Magnetic Properties of the New Ternary Nitride BaHfN2 and of the BaHf1–xZrxN2 Solid Solution. *J. Solid State Chem.* **1998**, *137* (1), 62–70.
- (75) Li, X.; Wang, X.; Han, Y.; Jing, X.; Huang, Q.; Kuang, X.; Gao, Q.; Chen, J.; Xing, X. High-Dielectric-Permittivity Layered Nitride CaTiN2. *Chem. Mater.* **2017**, *29* (5), 1989–1993.
- (76) Lenčič, Z.; Hirao, K.; Yamauchi, Y.; Kanzaki, S. Reaction Synthesis of Magnesium Silicon Nitride Powder. *J. Am. Ceram. Soc.* **2003**, *86* (7), 1088–1093.
- (77) Häusler, J.; Niklaus, R.; Minár, J.; Schnick, W. Ammonothermal Synthesis and Optical Properties of Ternary Nitride Semiconductors Mg-IV-N2, Mn-IV-N2 and Li-IV2-N3 (IV = Si, Ge). *Chem. Eur. J.* **2018**, *24* (7), 1686–1693.
- (78) Häusler, J.; Schimmel, S.; Wellmann, P.; Schnick, W. Ammonothermal Synthesis of Earth-Abundant Nitride Semiconductors ZnSiN2 and ZnGeN2 and Dissolution Monitoring by In Situ X-Ray Imaging. *Chem. - A Eur. J.* **2017**, *23* (50), 12275–12282.
- (79) Yamane, H.; DiSalvo, F. J. Sodium Flux Synthesis of Nitrides. *Prog. Solid State Chem.* **2018**, *51*, 27–40.
- (80) Misaki, T.; Wakahara, A.; Okada, H.; Yoshida, A. Epitaxial Growth and Characterization of ZnGeN2 by Metalorganic Vapor Phase Epitaxy. *J. Cryst. Growth* **2004**, *260* (1–2), 125–129.
- (81) Kikkawa, S.; Morisaka, H. RF-Sputter Deposition of Zn–Ge Nitride Thin Films. *Solid State Commun.* **1999**, *112* (9), 513–515.
- (82) Quayle, P. C.; Blanton, E. W.; Punya, A.; Junno, G. T.; He, K.; Han, L.; Zhao, H.; Shan, J.; Lambrecht, W. R. L.; Kash, K. Charge-Neutral Disorder and Polytypes in Heterovalent Wurtzite-Based Ternary Semiconductors: The Importance of the Octet Rule. *Phys. Rev. B* **2015**, *91* (20), 205207.
- (83) Lany, S.; Fioretti, A. N.; Zawadzki, P. P.; Schelhas, L. T.; Toberer, E. S.; Zakutayev, A.; Tamboli, A. C. Monte Carlo Simulations of Disorder in ZnSnN2 and the Effects on the Electronic Structure. *Phys. Rev. Mater.* **2017**, *1* (3), 035401.
- (84) Melamed, C. L.; Pan, J.; Mis, A.; Heinselman, K.; Schnepf, R. R.; Woods-Robinson, R.; Cordell, J. J.; Lany, S.; Toberer, E. S.; Tamboli, A. C. Combinatorial Investigation of Structural and Optical Properties of Cation-Disordered ZnGeN2. *J. Mater. Chem. C* **2020**, *8* (26), 8736–8746.
- (85) Kawamura, F.; Yamada, N.; Imai, M.; Taniguchi, T. Synthesis of ZnSnN2 Crystals via a High-Pressure Metathesis Reaction. *Cryst. Res. Technol.* **2016**, *51* (3), 220–224.
- (86) Kawamura, F.; Imura, M.; Murata, H.; Yamada, N.; Taniguchi, T. Synthesis of a Novel Rocksalt-Type Ternary Nitride Semiconductor MgSnN2 Using the Metathesis Reaction Under High Pressure. *Eur. J. Inorg. Chem.* **2020**, *2020*, 446.
- (87) Fioretti, A. N.; Zakutayev, A.; Moutinho, H.; Melamed, C.; Perkins, J. D.; Norman, A. G.; Al-Jassim, M.; Toberer, E. S.; Tamboli, A. C. Combinatorial Insights into Doping Control and Transport Properties of Zinc Tin Nitride. *J. Mater. Chem. C* **2015**, *3* (42), 11017–11028.
- (88) Greenaway, A. L.; Loutris, A. L.; Heinselman, K. N.; Melamed, C. L.; Schnepf, R. R.; Tellekamp, M. B.; Woods-Robinson, R.; Sherbondy, R.; Bardgett, D.; Bauers, S.; Zakutayev, A.; Christensen, S. T.; Lany, S.; Tamboli, A. C. Combinatorial Synthesis of Magnesium Tin Nitride Semiconductors. *J. Am. Chem. Soc.* **2020**, *142*, 8421.
- (89) Woods-Robinson, R.; Stevanović, V.; Lany, S.; Heinselman, K.; Persson, K. A.; Zakutayev, A. The Role of Disorder in the Synthesis of Metastable Ternary Nitrides. *arXiv*, **2020**, 2012.12455.
- (90) Orisakwe, E.; Fontaine, B.; Gregory, D. H.; Gautier, R.; Halet, J. F. Theoretical Study on the Structural, Electronic and Physical Properties of Layered Alkaline-Earth-Group-4 Transition-Metal Nitrides AEMN2. *RSC Adv.* **2014**, *4* (60), 31981–31987.
- (91) Hautier, G.; Fischer, C.; Ehrlicher, V.; Jain, A.; Ceder, G. Data Mined Ionic Substitutions for the Discovery of New Compounds. *Inorg. Chem.* **2011**, *50* (2), 656–663.

- (92) Sun, W.; Holder, A.; Orvañanos, B.; Arca, E.; Zakutayev, A.; Lany, S.; Ceder, G. Thermodynamic Routes to Novel Metastable Nitrogen-Rich Nitrides. *Chem. Mater.* **2017**, *29* (16), 6936.
- (93) Sun, J.; Ruzsinszky, A.; Perdew, J. Strongly Constrained and Appropriately Normed Semilocal Density Functional. *Phys. Rev. Lett.* **2015**, *115* (3), 036402.
- (94) Kong, Y.; Song, Z.; Wang, S.; Xia, Z.; Liu, Q. Charge Transfer, Local Structure, and the Inductive Effect in Rare-Earth-Doped Inorganic Solids. *Inorg. Chem.* **2018**, *57* (19), 12376–12383.
- (95) Zakutayev, A.; Allen, A. J.; Zhang, X.; Vidal, J.; Cui, Z.; Lany, S.; Yang, M.; Disalvo, F. J.; Ginley, D. S. Experimental Synthesis and Properties of Metastable CuNbN₂ and Theoretical Extension to Other Ternary Copper Nitrides. *Chem. Mater.* **2014**, *26* (17), 4970–4977.
- (96) Zhang, X.; Yu, L.; Zakutayev, A.; Zunger, A. Sorting Stable versus Unstable Hypothetical Compounds: The Case of Multi-Functional ABX Half-Heusler Filled Tetrahedral Structures. *Adv. Funct. Mater.* **2012**, *22* (7), 1425–1435.
- (97) Davies, D. W.; Butler, K. T.; Isayev, O.; Walsh, A. Materials Discovery by Chemical Analogy: Role of Oxidation States in Structure Prediction. *Faraday Discuss.* **2018**, *211* (0), 553–568.
- (98) Zhang, X.; Stevanović, V.; D’Avezac, M.; Lany, S.; Zunger, A. Prediction of A 2BX 4 Metal-Chalcogenide Compounds via First-Principles Thermodynamics. *Phys. Rev. B - Condens. Matter Mater. Phys.* **2012**, *86* (1), 014109.
- (99) Oganov, A. R.; Glass, C. W. Crystal Structure Prediction Using Ab Initio Evolutionary Techniques: Principles and Applications. *J. Chem. Phys.* **2006**, *124* (24), 244704.
- (100) Trimarchi, G.; Zunger, A. Global Space-Group Optimization Problem: Finding the Stablest Crystal Structure without Constraints. *Phys. Rev. B* **2007**, *75* (10), 104113.
- (101) Wang, Y.; Lv, J.; Zhu, L.; Ma, Y. CALYPSO: A Method for Crystal Structure Prediction. *Comput. Phys. Commun.* **2012**, *183* (10), 2063–2070.
- (102) Pickard, C. J.; Needs, R. J. Ab Initio Random Structure Searching. *J. Phys.: Condens. Matter* **2011**, *23* (5), 053201.
- (103) Wales, D. J.; Doye, J. P. K. Global Optimization by Basin-Hopping and the Lowest Energy Structures of Lennard-Jones Clusters Containing up to 110 Atoms. *J. Phys. Chem. A* **1997**, *101* (28), 5111–5116.
- (104) Burnham, C. J.; English, N. J. Crystal Structure Prediction via Basin-Hopping Global Optimization Employing Tiny Periodic Simulation Cells, with Application to Water–Ice. *J. Chem. Theory Comput.* **2019**, *15* (6), 3889–3900.
- (105) Lany, S. Semiconducting Transition Metal Oxides. *J. Phys.: Condens. Matter* **2015**, *27* (28), 283203.
- (106) Paudel, T. R.; Lambrecht, W. R. L. First-Principles Calculations of Elasticity, Polarization-Related Properties, and Nonlinear Optical Coefficients in Zn-IV- N₂ Compounds. *Phys. Rev. B* **2009**, *79* (24), 245205.
- (107) Punya, A.; Lambrecht, W. R. L.; Van Schilfgaarde, M. Quasiparticle Band Structure of Zn-IV-N₂ Compounds. *Phys. Rev. B* **2011**, *84* (16), 165204.
- (108) Tholander, C.; Andersson, C. B. A.; Armiento, R.; Tasnádi, F.; Alling, B. Strong Piezoelectric Response in Stable TiZnN₂, ZrZnN₂, and HfZnN₂ Found by Ab Initio High-Throughput Approach. *J. Appl. Phys.* **2016**, *120* (22), 225102.
- (109) Alling, B. Metal to Semiconductor Transition and Phase Stability of Ti1-XMgxNy Alloys Investigated by First-Principles Calculations. *Phys. Rev. B* **2014**, *89* (8), 85112.
- (110) Irokawa, Y.; Usami, M. First-Principles Calculations of Semiconducting TiMgN₂. *Jpn. J. Appl. Phys.* **2016**, *55* (9), 098001.
- (111) Heinselman, K. N.; Lany, S.; Perkins, J. D.; Talley, K. R.; Zakutayev, A. Thin Film Synthesis of Semiconductors in the Mg-Sb-N Materials System. *Chem. Mater.* **2019**, *31* (21), 8717–8724.
- (112) van de Walle, A.; Ceder, G. The Effect of Lattice Vibrations on Substitutional Alloy Thermodynamics. *Rev. Mod. Phys.* **2002**, *74* (1), 11.
- (113) Sanchez, J. M.; Ducastelle, F.; Gratias, D. Generalized Cluster Description of Multicomponent Systems. *Phys. A Stat. Mech. its Appl.* **1984**, *128* (1–2), 334–350.
- (114) Blum, V.; Zunger, A. Mixed-Basis Cluster Expansion for Thermodynamics of Bcc Alloys. *Phys. Rev. B* **2004**, *70* (15), 155108.
- (115) Van de Walle, A.; Asta, M.; Ceder, G. The Alloy Theoretic Automated Toolkit: A User Guide. *Calphad* **2002**, *26* (4), 539–553.
- (116) Cordell, J. J.; Pan, J.; Tamboli, A. C.; Tucker, G. J.; Lany, S. Probing Configurational Disorder in ZnGeN₂ Using Cluster-Based Monte Carlo. *Phys. Rev. Mater.* **2021**, *5* (2), 024604.
- (117) Ferreyra, R. A.; Zhu, C.; Teke, A.; Morkoç, H. *Group III Nitrides*; Springer: 2017; .
- (118) Caldwell, J. D.; Aharonovich, I.; Cassabois, G.; Edgar, J. H.; Gil, B.; Basov, D. N. Photonics with Hexagonal Boron Nitride. *Nat. Rev. Mater.* **2019**, *4* (8), 552–567.
- (119) Dismukes, J. P.; Smith, R. T.; White, J. G. Physical Properties and Crystal Structure of a New Semiconducting I–III–VI₂ Compound, CuScS₂. *J. Phys. Chem. Solids* **1971**, *32* (5), 913–922.
- (120) Scanlon, D. O.; Watson, G. W. Stability, Geometry, and Electronic Structure of an Alternative I-III-VI₂ Material, CuScS₂: A Hybrid Density Functional Theory Analysis. *Appl. Phys. Lett.* **2010**, *97* (13), 131904.
- (121) Meng, Y.; Mao, H. K.; Eng, P. J.; Trainor, T. P.; Newville, M.; Hu, M. Y.; Kao, C.; Shu, J.; Hausermann, D.; Hemley, R. J. The Formation of Sp³ Bonding in Compressed BN. *Nat. Mater.* **2004**, *3* (2), 111–114.
- (122) Wang, H.; Li, Q.; Cui, T.; Ma, Y.; Zou, G. Phase-Transition Mechanism of h-BN → w-BN from First Principles. *Solid State Commun.* **2009**, *149* (21–22), 843–846.
- (123) Limpijumnong, S.; Lambrecht, W. R. L. Homogeneous Strain Deformation Path for the Wurtzite to Rocksalt High-Pressure Phase Transition in GaN. *Phys. Rev. Lett.* **2001**, *86* (1), 91–94.
- (124) Xia, H.; Xia, Q.; Ruoff, A. L. High-Pressure Structure of Gallium Nitride: Wurtzite-to-Rocksalt Phase Transition. *Phys. Rev. B* **1993**, *47* (19), 12925–12928.
- (125) Range, K. J.; Engert, G.; Weiss, A. Darstellung Und Kristallstruktur Der Hochdruckphase AgAlS₂-II. *Zeitschrift fur Naturforsch.* **1974**, *29* (3–4), 186–189.
- (126) Frazer, E. J.; Phang, S. Titanium Disulphide as a Cathode Material in Lithium Batteries - a Review. *J. Power Sources* **1981**, *6* (4), 307–317.
- (127) Huang, Y.; Sutter, E.; Sadowski, J. T.; Cotlet, M.; Monti, O. L. A.; Racke, D. A.; Neupane, M. R.; Wickramaratne, D.; Lake, R. K.; Parkinson, B. A.; Sutter, P. Tin Disulfide-an Emerging Layered Metal Dichalcogenide Semiconductor: Materials Properties and Device Characteristics. *ACS Nano* **2014**, *8* (10), 10743–10755.
- (128) Zhao, R.; Grisafe, B.; Ghosh, R. K.; Holoviak, S.; Wang, B.; Wang, K.; Briggs, N.; Haque, A.; Datta, S.; Robinson, J. Two-Dimensional Tantalum Disulfide: Controlling Structure and Properties via Synthesis. *2D Mater.* **2018**, *5* (2), 025001.
- (129) Wieggers, G. A.; Haange, R. J.; van Bolhuis, F. The Crystal Structure of Stage-2 4H Ag_{0.22}NbS₂. *Phys. Status Solidi* **1988**, *107* (2), 817–824.
- (130) Boswell, F. W.; Prodan, A.; Corbett, J. M. Investigation of Order in Ag_xNbS₂ by Electron Diffraction. *Mater. Res. Bull.* **1980**, *15* (11), 1567–1574.
- (131) Li, Z.; Meng, X.; Zhang, Z. Recent Development on MoS₂-Based Photocatalysis: A Review. *J. Photochem. Photobiol. C* **2018**, *35*, 39–55.
- (132) Cao, J.; Li, T.; Gao, H.; Lin, Y.; Wang, X.; Wang, H.; Palacios, T.; Ling, X. Realization of 2D Crystalline Metal Nitrides via Selective Atomic Substitution. *Sci. Adv.* **2020**, *6* (2), eaax8784.
- (133) Chalcogenides Fill the Gap. *Nat. Mater.* **2014**, *13* (12), 1073; .
- (134) Tominaga, J.; Kolobov, A. V. *Two-Dimensional Transition-Metal Dichalcogenides*; Springer: 2016.
- (135) Whittingham, M. S. Electrical Energy Storage and Intercalation Chemistry. *Science (80-)* **1976**, *192* (4244), 1126–1127.
- (136) Verrelli, R.; Arroyo-de-Dompablo, M. E.; Tchitchekova, D.; Black, A. P.; Frontera, C.; Fuertes, A.; Palacin, M. R. On the Viability of

Mg Extraction in MgMoN₂: A Combined Experimental and Theoretical Approach. *Phys. Chem. Chem. Phys.* **2017**, *19* (38), 26435–26441.

(137) Pauling, L. The Principles Determining the Structure of Complex Ionic Crystals. *J. Am. Chem. Soc.* **1929**, *51* (4), 1010–1026.

(138) Burdett, J. K.; Price, G. D.; Price, S. L. Factors Influencing Solid-State Structure Analysis Using Pseudopotential Radii Structural Maps. *Phys. Rev. B* **1981**, *24* (6), 2903–2912.

(139) Phillips, J. C. Bonds and Bands in Semiconductors. *Science* (80-) **1970**, *169* (3950), 1035–1042.

(140) Xue, F.; Sun, M.; Feng, X.; Lu, Y.; Zhang, J. Electronic Structure, Dynamic Stability, Elastic, and Optical Properties of MgTMN₂ (TM = Ti, Zr, Hf) Ternary Nitrides from First-Principles Calculations. *J. Appl. Phys.* **2021**, *129* (13), 135103.

(141) Ward, L.; Liu, R.; Krishna, A.; Hegde, V. I.; Agrawal, A.; Choudhary, A.; Wolverton, C. Including Crystal Structure Attributes in Machine Learning Models of Formation Energies via Voronoi Tessellations. *Phys. Rev. B* **2017**, *96* (2), 24104.

(142) Xie, T.; Grossman, J. C. Crystal Graph Convolutional Neural Networks for an Accurate and Interpretable Prediction of Material Properties. *Phys. Rev. Lett.* **2018**, *120* (14), 145301.

(143) Veal, T. D.; Feldberg, N.; Quackenbush, N. F.; Linhart, W. M.; Scanlon, D. O.; Piper, L. F. J.; Durbin, S. M. Band Gap Dependence on Cation Disorder in ZnSnN₂ Solar Absorber. *Adv. Energy Mater.* **2015**, *5* (24), 1501462.

(144) Baranowski, L. L.; Zawadzki, P.; Lany, S.; Toberer, E. S.; Zakutayev, A. A Review of Defects and Disorder in Multinary Tetrahedrally Bonded Semiconductors. *Semicond. Sci. Technol.* **2016**, *31* (12), 123004.

(145) Schorr, S.; Gurieva, G.; Guc, M.; Dimitrievska, M.; Pérez-Rodríguez, A.; Izquierdo-Roca, V.; Schnohr, C. S.; Kim, J.; Jo, W.; Merino, J. M. Point Defects, Compositional Fluctuations, and Secondary Phases in Non-Stoichiometric Kesterites. *J. Phys. Energy* **2020**, *2* (1), 012002.

(146) Fioretti, A. N.; Stokes, A.; Young, M. R.; Gorman, B.; Toberer, E. S.; Tamboli, A. C.; Zakutayev, A. Effects of Hydrogen on Acceptor Activation in Ternary Nitride Semiconductors. *Adv. Electron. Mater.* **2017**, *3* (3), 1600544.

(147) Melamed, C. L.; Tellekamp, M. B.; Mangum, J. S.; Perkins, J. D.; Dippo, P.; Toberer, E. S.; Tamboli, A. C. Blue-Green Emission from Epitaxial yet Cation-Disordered ZnGeN₂-XOx. *Phys. Rev. Mater.* **2019**, *3* (5), 51602.

(148) Kresse, G.; Joubert, D. From Ultrasoft Pseudopotentials to the Projector Augmented-Wave Method. *Phys. Rev. B* **1999**, *59* (3), 1758–1775.

(149) Arca, E.; Perkins, J. D.; Lany, S.; Mis, A.; Chen, B. R.; Dippo, P.; Partridge, J. L.; Sun, W.; Holder, A.; Tamboli, A. C.; Toney, M. F.; Schelhas, L. T.; Ceder, G.; Tumas, W.; Teeter, G.; Zakutayev, A. Zn₂SbN₃: Growth and Characterization of a Metastable Photoactive Semiconductor. *Mater. Horizons* **2019**, *6* (8), 1669–1674.

(150) Mis, A.; Lany, S.; Brennecke, G. L.; Tamboli, A. Exploring the Phase Space of Zn₂SbN₃, a Novel Semiconducting Nitride. *J. Mater. Chem. C* **2021**, *9* (39), 13904–13913.

(151) Cordell, J. J.; Tucker, G. J.; Tamboli, A. C.; Lany, S. Role of Cation Disorder in Carrier Localization and Density of States in ZnGeN₂. *arXiv*, 2021, 2109.05062.

(152) Ndione, P. F.; Shi, Y.; Stevanovic, V.; Lany, S.; Zakutayev, A.; Parilla, P. A.; Perkins, J. D.; Berry, J. J.; Ginley, D. S.; Toney, M. F. Control of the Electrical Properties in Spinel Oxides by Manipulating the Cation Disorder. *Adv. Funct. Mater.* **2014**, *24* (5), 610–618.

(153) Blanton, E. W.; He, K.; Shan, J.; Kash, K. Characterization and Control of ZnGeN₂ Cation Lattice Ordering. *J. Cryst. Growth* **2017**, *461*, 38–45.

(154) Zunger, A.; Wei, S.-H.; Ferreira, L. G.; Bernard, J. E. Special Quasirandom Structures. *Phys. Rev. Lett.* **1990**, *65* (3), 353.

(155) Biswas, K.; Lany, S. Energetics of Quaternary III-V Alloys Described by Incorporation and Clustering of Impurities. *Phys. Rev. B* **2009**, *80* (11), 115206.

(156) Pan, J.; Cordell, J. J.; Tucker, G. J.; Zakutayev, A.; Tamboli, A. C.; Lany, S. Perfect Short-Range Ordered Alloy with Line-Compound-like Properties in the ZnSnN₂:ZnO System. *npj Comput. Mater.* **2020**, *6* (1), 1–6.

(157) Fioretti, A. N.; Pan, J.; Ortiz, B. R.; Melamed, C. L.; Dippo, P. C.; Schelhas, L. T.; Perkins, J. D.; Kuciauskas, D.; Lany, S.; Zakutayev, A.; Toberer, E. S.; Tamboli, A. C. Exciton Photoluminescence and Benign Defect Complex Formation in Zinc Tin Nitride. *Mater. Horizons* **2018**, *5* (5), 823–830.

(158) Urban, A.; Abdellahi, A.; Dacek, S.; Artrith, N.; Ceder, G. Electronic-Structure Origin of Cation Disorder in Transition-Metal Oxides. *Phys. Rev. Lett.* **2017**, *119* (17), 176402.

(159) Todd, P. K.; Fallon, M. J.; Neilson, J. R.; Zakutayev, A. Two-Step Solid-State Synthesis of Ternary Nitride Materials. *ACS Mater. Lett.* **2021**, *3*, 1677–1683.

(160) Bauers, S. R.; Hamann, D. M.; Patterson, A.; Perkins, J. D.; Talley, K. R.; Zakutayev, A. Composition, Structure, and Semiconducting Properties of Mg x Zr₂-Xn₂ Thin Films. *Jpn. J. Appl. Phys.* **2019**, *58* (SC), SC1015.

(161) Fioretti, A. N.; Zakutayev, A.; Moutinho, H.; Melamed, C.; Perkins, J. D.; Norman, A. G.; Al-Jassim, M.; Toberer, E. S.; Tamboli, A. C. Combinatorial Insights into Doping Control and Transport Properties of Zinc Tin Nitride. *J. Mater. Chem. C* **2015**, *3* (42), 11017–11028.

(162) Tsuji, M.; Hanzawa, K.; Kinjo, H.; Hiramatsu, H.; Hosono, H. Heteroepitaxial Thin-Film Growth of a Ternary Nitride Semiconductor CaZn₂N₂. *ACS Appl. Electron. Mater.* **2019**, *1* (8), 1433–1438.

(163) Kikuchi, R.; Ueno, K.; Nakamura, T.; Kurabuchi, T.; Kaneko, Y.; Kumagai, Y.; Oba, F. SrZn₂N₂ as a Solar Absorber: Theoretical Defect Chemistry and Synthesis by Metal Alloy Nitridation. *Chem. Mater.* **2021**, *33* (8), 2864–2870.

(164) Tsuji, M.; Hiramatsu, H.; Hosono, H. Tunable Light Emission through the Range 1.8–3.2 eV and p-Type Conductivity at Room Temperature for Nitride Semiconductors, Ca(Mg_{1-x}Zn_x)₂N₂ (x = 0–1). *Inorg. Chem.* **2019**, *58* (18), 12311–12316.

(165) Kikuchi, R.; Nakamura, T.; Kurabuchi, T.; Kaneko, Y.; Kumagai, Y.; Oba, F. Theoretical Prediction and Thin-Film Growth of the Defect-Tolerant Nitride Semiconductor YZn₃N₃. *Chem. Mater.* **2021**, *33*, 8205.

(166) Richter, T. M. M.; Niewa, R. Chemistry of Ammonothermal Synthesis. *Inorganics* **2014**, *2* (1), 29–78.

(167) Kloß, S. D.; Schnick, W. Nitridophosphates: A Success Story of Nitride Synthesis. *Angew. Chemie - Int. Ed.* **2019**, *58* (24), 7933–7944.

(168) Häusler, J.; Niklaus, R.; Minár, J.; Schnick, W. Ammonothermal Synthesis and Optical Properties of Ternary Nitride Semiconductors Mg-IV-N₂, Mn-IV-N₂ and Li-IV₂-N₃ (IV = Si, Ge). *Chem. - A Eur. J.* **2018**, *24* (7), 1686–1693.

(169) Matthews, B. E. Synthesis and Analysis of Heterostructural Semiconductor Alloy Sn_{1-x}CaxCh (Ch = S, Se) and Nitrides Zn_{1-x}WxN and Zn_{1-x}(W_{1-y}Moy)_xN. Ph.D. Thesis, Oregon State University, 2018.

(170) Kim, J.; Bauers, S. R.; Khan, I. S.; Perkins, J.; Park, B. I.; Talley, K. R.; Kim, D.; Zakutayev, A.; Shin, B. Influence of Hydrogen and Oxygen on the Structure and Properties of Sputtered Magnesium Zirconium Oxynitride Thin Films. *J. Mater. Chem. A* **2020**, *8* (18), 9364–9372.

(171) Chi, E. O.; Kim, W. S.; Hur, N. H.; Jung, D. New Mg-Based Antiperovskites PnNMg₃ (Pn = As, Sb). *Solid State Commun.* **2002**, *121* (6–7), 309–312.

(172) Jansen, M. Crystal Structure of Sb₂O₅. *Angew. Chemie Int. Ed.* **1978**, *17* (2), 137–137.

(173) Allen, J. P.; Carey, J. J.; Walsh, A.; Scanlon, D. O.; Watson, G. W. Electronic Structures of Antimony Oxides. *J. Phys. Chem. C* **2013**, *117* (28), 14759–14769.

(174) Zakutayev, A.; Perkins, C. L. Influence of Protection Layers on Thermal Stability of Nitride Thin Films. *Phys. Status Solidi - Rapid Res. Lett.* **2021**, *15* (8), 2100178.

(175) Zhuk, S.; Kistanov, A. A.; Boehme, S. C.; Ott, N.; Stiefel, M.; Kovalenko, M. V.; Siol, S. Synthesis of a New Ternary Nitride

Semiconductor -- Zn₂VN₃: A Combinatorial Exploration of the Zn-V-N Phase Space. *arXiv*, 2021, 2109.00365.

(176) Fenker, M.; Balzer, M.; Kappl, H.; Banakh, O. Some Properties of (Ti,Mg)N Thin Films Deposited by Reactive Dc Magnetron Sputtering. *Surf. Coat. Technol.* **2005**, *200* (1–4), 227–231.

(177) Wang, B.; Gall, D. Fully Strained Epitaxial Ti_{1-x}MgxN(001) Layers. *Thin Solid Films* **2019**, *688*, 137165.

(178) Wang, B.; Kerdsonpanya, S.; McGahay, M. E.; Milosevic, E.; Patsalas, P.; Gall, D. Growth and Properties of Epitaxial Ti_{1-x}Mg_xN(001) Layers. *J. Vac. Sci. Technol. A* **2018**, *36* (6), 061501.

(179) Gharavi, M. A.; le Febvrier, A.; Lu, J.; Greczynski, G.; Alling, B.; Armiento, R.; Eklund, P. Phase Transformation and Superstructure Formation in (Ti_{0.5},Mg_{0.5})N Thin Films through High-Temperature Annealing. *Coatings* **2021**, *11* (1), 89.

(180) Wang, B.; Nawarat, P.; Lewis, K. M.; Patsalas, P.; Gall, D. Tunable Infrared Plasmonic Properties of Epitaxial Ti_{1-x}MgxN(001) Layers. *ACS Appl. Mater. Interfaces* **2021**, *13* (19), 22738–22748.

(181) Wang, L.; Tang, K.; Zhu, Y.; Li, Q.; Zhu, B.; Wang, L.; Si, L.; Qian, Y. Solid State Synthesis of a New Ternary Nitride MgMoN₂ Nanosheets and Micromeshes. *J. Mater. Chem.* **2012**, *22* (29), 14559–14564.

(182) Brokamp, T.; Jacobs, H. Darstellung Und Struktur Einiger Gemischtvalenter Ternärer Tantalnitride Mit Lithium Und Magnesium. *J. Alloys Compd.* **1992**, *183* (C), 325–344.

(183) Rom, C. L.; Fallon, M. J.; Wustrow, A.; Prieto, A. L.; Neilson, J. R. Bulk Synthesis, Structure, and Electronic Properties of Magnesium Zirconium Nitride Solid Solutions. *Chem. Mater.* **2021**, *33* (13), 5345–5354.

(184) Bauers, S. R.; Mangum, J.; Harvey, S. P.; Perkins, J. D.; Gorman, B.; Zakutayev, A. Epitaxial Growth of Rock Salt MgZrN₂ Semiconductors on MgO and GaN. *Appl. Phys. Lett.* **2020**, *116*, 102102.

(185) Wachsmann, C.; Brokamp, T.; Jacobs, H. Darstellung Und Struktur Eines Neuen Nitridoxides Mit Lithium Und Tantal: Li₁₆Ta₂N₈O. *J. Alloys Compd.* **1992**, *185* (1), 109–119.

(186) Wu, Q.; Piveteau, C.; Song, Z.; Yazyev, O. V. MgTa₂N₃: A Reference Dirac Semimetal. *Phys. Rev. B* **2018**, *98* (8), 081115.

(187) Huang, H.; Jin, K. H.; Liu, F. Alloy Engineering of Topological Semimetal Phase Transition in MgTa₂-XNbx N₃. *Phys. Rev. Lett.* **2018**, *120* (13), 136403.

(188) Stevanović, V. Sampling Polymorphs of Ionic Solids Using Random Superlattices. *Phys. Rev. Lett.* **2016**, *116* (7), 075503.

(189) Rognerud, E. G.; Rom, C. L.; Todd, P. K.; Singstock, N. R.; Bartel, C. J.; Holder, A. M.; Neilson, J. R. Kinetically Controlled Low-Temperature Solid-State Metathesis of Manganese Nitride Mn₃N₂. *Chem. Mater.* **2019**, *31* (18), 7248–7254.

(190) Mori, Y.; Imade, M.; Maruyama, M.; Yoshimura, M.; Yamane, H.; Kawamura, F.; Kawamura, T. Growth of Bulk Nitrides from a Na Flux. In *Handbook of Crystal Growth: Bulk Crystal Growth*, 2nd ed.; Elsevier Inc.: 2015; Vol. 2, pp 505–533; .

(191) Hamilton, D. C.; Arca, E.; Pan, J.; Siol, S.; Young, M.; Lany, S.; Zakutayev, A. Electron Scattering Mechanisms in Polycrystalline Sputtered Zinc Tin Oxynitride Thin Films. *J. Appl. Phys.* **2019**, *126* (3), 035701.

(192) Bem, D. S.; Lampe-Önnerud, C. M.; Olsen, H. P.; zur Loye, H.-C. Synthesis and Structure of Two New Ternary Nitrides: FeWN₂ and MnMoN₂. *Inorg. Chem.* **1996**, *35* (3), 581–585.

(193) Kim, K. K.; Lee, H. S.; Lee, Y. H. Synthesis of Hexagonal Boron Nitride Heterostructures for 2D van Der Waals Electronics. *Chem. Soc. Rev.* **2018**, *47* (16), 6342–6369.

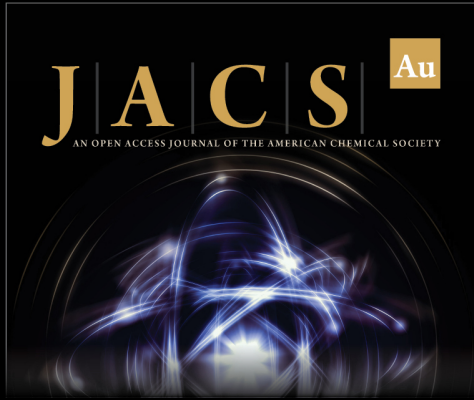
(194) Martinolich, A. J.; Neilson, J. R. Toward Reaction-by-Design: Achieving Kinetic Control of Solid State Chemistry with Metathesis. *Chem. Mater.* **2017**, *29* (2), 479–489.

(195) Shoemaker, D. P.; Hu, Y. J.; Chung, D. Y.; Halder, G. J.; Chupas, P. J.; Soderholm, L.; Mitchell, J. F.; Kanatzidis, M. G. In Situ Studies of a Platform for Metastable Inorganic Crystal Growth and Materials Discovery. *Proc. Natl. Acad. Sci. U. S. A.* **2014**, *111* (30), 10922–10927.

(196) Dolique, V.; Jaouen, M.; Cabioch, T.; Pailloux, F.; Gúrin, P.; Pélosin, V. Formation of (Ti,Al)N/Ti₂AlN Multilayers after Annealing


of TiN/TiAl(N) Multilayers Deposited by Ion Beam Sputtering. *J. Appl. Phys.* **2008**, *103* (8), 083527.


(197) Höglund, C.; Beckers, M.; Schell, N.; Borany, J. V.; Birch, J.; Hultman, L. Topotaxial Growth of Ti₂AlN by Solid State Reaction in AlN/Ti(0001) Multilayer Thin Films. *Appl. Phys. Lett.* **2007**, *90* (17), 174106.



JACS Au
AN OPEN ACCESS JOURNAL OF THE AMERICAN CHEMICAL SOCIETY

Editor-in-Chief
Prof. Christopher W. Jones
Georgia Institute of Technology, USA

Open for Submissions 

pubs.acs.org/jacsau  ACS Publications
Most Trusted. Most Cited. Most Read.